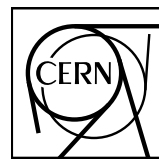


EUROPEAN ORGANIZATION FOR NUCLEAR RESEARCH



CERN-EP-2025-096
22 April 2025

Femtoscopic study of the proton-proton and proton-deuteron systems in heavy-ion collisions at the LHC

ALICE Collaboration*

Abstract

This work reports femtoscopic correlations of p-p ($\bar{p}-\bar{p}$) and p-d ($\bar{p}-\bar{d}$) pairs measured in Pb-Pb collisions at center-of-mass energy $\sqrt{s_{NN}} = 5.02$ TeV by the ALICE Collaboration. A fit to the measured proton-proton correlation functions allows one to extract the dependence of the nucleon femtoscopic radius of the particle-emitting source on the pair transverse mass (m_T) and on the average charge particle multiplicity $\langle dN_{ch}/d\eta \rangle^{1/3}$ for three centrality intervals (0–10%, 10–30%, 30–50%). In both cases, the expected power-law and linear scalings are observed, respectively. The measured p-d correlations can be described by both two- and three-body calculations, indicating that the femtoscopy observable is not sensitive to the short-distance features of the dynamics of the p-(p-n) system, due to the large inter-particle distances in Pb-Pb collisions at the LHC. Indeed, in this study, the minimum measured femtoscopic source sizes for protons and deuterons have a minimum value at $2.73^{+0.05}_{-0.05}$ and $3.10^{+1.04}_{-0.86}$ fm, respectively, for the 30–50% centrality collisions. Moreover, the m_T -scaling obtained for the p-p and p-d systems is compatible within 1σ of the uncertainties. These findings provide new input for fundamental studies on the production of light (anti)nuclei under extreme conditions.

© 2025 CERN for the benefit of the ALICE Collaboration.

Reproduction of this article or parts of it is allowed as specified in the CC-BY-4.0 license.

*See Appendix A for the list of collaboration members

1 Introduction

The energy density reached in ultra-relativistic heavy-ion collisions (HICs) allows for the production of short-lived droplets made of deconfined quarks and gluons [1–8]. This state of matter, called the quark–gluon plasma (QGP), evolves in approximately $10 \text{ fm}/c$ [9, 10] into final-state particles through the hadronization process, after which the quarks and gluons are confined inside hadrons [11].

In HICs, statistical hadronization models (SHMs) [12, 13] can well reproduce the production yields of abundant hadron species such as π and p , as well as light ions and particles containing heavier quarks, e.g., d , ${}^3\text{He}$, K , Λ , and ϕ . These models describe the system that undergoes hadronization at a chemical potential close to zero and a temperature of approximately $156 \pm 9 \text{ MeV}$ [14]. This temperature value is also predicted by lattice quantum chromodynamics calculations [15] for the cross-over of the QGP system into a hadronic system. It is surprising that the models also work well in predicting the yield of nucleon-based composite objects, such as deuterons and other light nuclei or even hypernuclei, despite the large difference between the temperatures that characterize the hadronization process and the binding energy of these particles. For example, the binding energy of the deuteron is 2.22 MeV [16], 70 times smaller than the chemical equilibrium temperature extracted employing the SHMs. Alternative descriptions of data on nuclei are based on the coalescence mechanism [17, 18]. It describes the formation of light nuclei in high-energy hadron collisions by combining nucleons that are close in phase space during the expansion of the fireball. Calculations based on the coalescence mechanism have shown significant success in reproducing experimental data on light-nucleus production from measurements conducted at the Large Hadron Collider (LHC) and the Relativistic Heavy Ion Collider (RHIC), demonstrating its effectiveness in capturing the dynamics of nuclear formation in HICs [19, 20].

In addition to the aforementioned spectra studies, light ion production mechanisms can be investigated through the measurement of elliptic flow, which is sensitive to the conditions in the early stages of the system evolution [20–23]. However, the elliptic flow distribution of deuterons could not be consistently reproduced across all centralities using only SHMs or the coalescence approach [23]. Additionally, the production of deuterons in HICs should be reflected in fluctuation measurements [24], the results of which have been well reproduced by SHMs but not by simple coalescence models. Despite the combined efforts across different observables, the overall understanding of deuteron production in collisions involving the QGP state remains ambiguous.

Furthermore, momentum correlations involving nuclei can be exploited to study the production mechanisms of light ions [25–28] by comparing their emission properties with those of abundant hadrons emitted in the collisions. Femtoscopy, which relies on analyzing momentum correlations between particles, is used to study the space-time properties of particle emission and to examine the final-state interactions (FSI) of the emitted hadrons [29]. Measurements carried out in HICs for particles which are formed directly in the hadronization process, such as π , K , and p [30–35], showed a linear dependence of the femtoscopic radii with the cube root of the mean charged-particle multiplicity [35–40] and a decreasing power-law dependence upon the pair transverse mass, m_T [35, 41]. For single particles, the latter is defined as $m_T = \sqrt{p_T^2 + m^2}$, where p_T is the particle's transverse momentum and m is its rest mass. For identical particle pairs, p_T in this expression is replaced by $k_T = |\mathbf{p}_{T,1} + \mathbf{p}_{T,2}|/2$, which is the average transverse momentum of the pair. The observed m_T -scaling is attributed to the radial flow of the collective expansion of the system driven by internal pressure. Indeed, these effects can be replicated by models that include a QGP phase described through relativistic hydrodynamic calculations [42–44]. A direct consequence of the hydrodynamic evolution of the system is the observation that the higher the transverse mass of the particle, the smaller the femtoscopic source size [45]. The common m_T -scaling has been observed for mesons and baryons such as π , K , and p both in pp and Pb–Pb collisions [35, 40, 40, 46, 47]. However, it remains an open question, whether light nuclei and hypernuclei follow the common m_T -scaling of the other hadrons.

This paper presents measurements of the space-time properties of the emission of nucleons and deuterons as a function of pair m_T based on the femtoscopy of two identical protons (p–p) and femtoscopy of proton–deuteron pairs (p–d). In both p–p and p–d analyses, three centrality intervals were chosen 0–10%, 10–30%, and 30–50%. The most precise measurements of p–p correlation functions in eight m_T ranges in Pb–Pb collisions at $\sqrt{s_{\text{NN}}} = 5.02$ TeV are presented, aimed at determining the m_T scaling of nucleon femtoscopic radii. The p–d correlations were then interpreted using two different models for the FSI [48, 49] to extract the corresponding single nucleon and deuteron source radii in two distinct m_T ranges. This analysis implies that deuterons follow the same m_T -scaling behavior observed for single nucleons.

2 Data analysis

The study is based on 337×10^6 Pb–Pb collisions at $\sqrt{s_{\text{NN}}} = 5.02$ TeV collected during the LHC Run 2 period (2018) with the ALICE detector [50, 51]. The main sub-detectors used in this work are the V0 detectors and three central barrel detectors: the Inner Tracking System (ITS) [52], the Time Projection Chamber (TPC) [53], and the Time-Of-Flight detector (TOF) [53]. The V0 detectors (V0A and V0C) [54] are located outside the central barrel on both sides of the interaction point. All the central barrel detectors are placed in a homogenous 0.5 T solenoidal magnetic field that is parallel to the beam direction.

The V0 detectors are utilized in the trigger system to determine the centrality of the collision. They consist of two arrays of scintillators, each comprising 32 scintillator counters, covering the pseudorapidity ranges of $2.8 < \eta < 5.1$ (V0A), and $-3.7 < \eta < -1.7$ (V0C). The minimum bias trigger for recording collision events requires that both V0 detectors register at least one hit simultaneously, coinciding with a collision occurring within a bunch crossing at the center of the ALICE detector. The centrality of the collision, expressed as a percentage of the total hadronic cross section, is determined based on the amplitudes of the signals left in both V0 arrays [55]. In this study, the collisions are classified into three intervals of the Pb–Pb cross section: 0–10%, 10–30%, and 30–50%. All centrality classes use events selected using the minimum bias trigger. In addition, the central and semi-central triggers [56] are used to enhance the statistical significance in 0–10% and 30–50% centrality intervals, respectively. To ensure uniform acceptance at midrapidity, only collisions occurring within ± 10 cm of the nominal interaction point along the beam axis are used in the study.

The ITS is a silicon detector made of six cylindrical layers used for precise primary vertex reconstruction. The TPC is the main tracking detector, used for momentum reconstruction and particle identification (PID) via specific energy-loss (dE/dx) measurement. It is a gas-filled cylindrical barrel, divided into two halves by a central cathode, with each half having its readout. Charged particles ionize the gas, producing drifting electrons that create signals in the pad rows of one of 18 azimuthal sectors. The TOF detector is also used in PID, as it can determine the mass hypothesis of a measured particle by combining its time-of-flight measurement with the expected trajectory length and momentum. It is shaped as a hollow cylinder surrounding the other detectors at a distance of about 380 cm from the center of the beam pipe. The TOF utilizes Multigap Resistive Plate Chamber (MRPC) detectors to measure the time at which charged particles cross its sensitive gas volume.

The PID is based on the evaluation of the absolute deviations from the signal hypotheses in units of the respective detector resolutions σ_{TPC} and σ_{TOF} at specific particle momentum. For this analysis, different transverse momentum (p_T) intervals were considered for the tracks, depending on the particle species. The p_T ranges are 0.5–3.0 GeV/c for (anti)protons and 0.8–2.0 GeV/c for (anti)deuterons. The (anti)proton candidates are selected by combining TPC and TOF signals, requiring $\sqrt{n_{\sigma,\text{TPC}}^2 + n_{\sigma,\text{TOF}}^2} < 3$. To ensure high-quality identification of (anti)deuterons, the strict criterion of $n_{\sigma,\text{TPC}} < 2$ is applied for momenta $p < 1.3$ GeV/c, while above this range, both $n_{\sigma,\text{TPC}} < 2$ and $n_{\sigma,\text{TOF}} < 2$ are employed simultaneously. The particles under study are identified in the pseudorapidity range $|\eta| < 0.8$. To reduce the contribution of (anti)protons and deuterons candidates originating from weak decays or knock-out

occurring in the interaction of particles with the detector material, the distance of the closest approach (DCA) to the primary vertex is required to be smaller than $0.0105 + 0.0350/(p_T/(\text{GeV}/c))^{1.1}$ cm in the transverse plane and 1 cm along the beam direction, as most secondary particles have larger DCAs. Since the contribution of (anti)deuterons originating from weak decays is negligible, and there are no secondary antideuterons from the material, antideuteron tracks are accepted if the DCA is smaller than 2.4 cm in the transverse plane and 3.2 cm along the beam direction.

Finally, the selected (anti)proton and (anti)deuteron candidates are combined to build proton–proton (p – p), antiproton–antiproton (\bar{p} – \bar{p}), proton–deuteron (p – d), and antiproton–antideuteron (\bar{p} – \bar{d}) pairs. To minimize detector effects, such as track merging, a similar approach based on a close-pair-rejection criterion [57] is applied when the relative pseudorapidity of the two tracks is less than 0.01 ($|\Delta\eta| < 0.01$). Pairs of tracks within the volume of the TPC are removed if their spatial overlap, defined as the percentage of points where the distance between two tracks in TPC is smaller than 3 cm, is above 5% and 2% for p – p and p – d study, respectively.

3 The femtoscopic correlation function

The femtoscopic correlation function, denoted as $C(k^*)$, is measured as a function of the relative momentum. Here, k^* is defined as $k^* = |\mathbf{p}_1^* - \mathbf{p}_2^*|/2$, where $\mathbf{p}_{1/2}^*$ are the particle momenta in the pair rest frame, indicated by the asterisk (*) notation. Experimentally, it is computed as

$$C_{\text{exp}}(k^*) = \mathcal{N} \frac{N_{\text{same}}(k^*)}{N_{\text{mixed}}(k^*)}, \quad (1)$$

where $N_{\text{same}}(k^*)$ is the correlated distribution of k^* , which is obtained from particle pairs originating in the same collision (same event), and $N_{\text{mixed}}(k^*)$ is the corresponding distribution of uncorrelated pairs. The latter is generated using the mixed-event technique [29], where pairs are built by selecting particles belonging to different events with similar primary vertex positions and collision centrality. The normalization term \mathcal{N} is used to scale the mixed-event distribution such that the integral over the selected range is equivalent to the analogous integral calculated for the same events. The \mathcal{N} factor is obtained within the range $k^* \in (300, 600)$ MeV/ c for p – p and p – d pairs. This interval is selected to ensure the absence of a femtoscopic signal, i.e. when $C(k^*)$ approaches unity. The number of pairs used in the analysis that contribute to the $k^* < 200$ MeV/ c interval, is summarized in Tab. 1.

Table 1: Number of p – p , \bar{p} – \bar{p} , p – d , and \bar{p} – \bar{d} pairs originating in the same collisions and contributing to the $k^* < 200$ MeV/ c interval.

Centrality	p – p	\bar{p} – \bar{p}	p – d	\bar{p} – \bar{d}
0-10%	1.5×10^8	9.0×10^7	6.0×10^4	2.8×10^4
10-30%	1.5×10^7	9.6×10^6	7.0×10^3	3.5×10^3
30-50%	1.2×10^7	7.2×10^6	5.6×10^3	3.0×10^3

The relation between the experimental $C_{\text{exp}}(k^*)$ and model $C_{\text{femto}}(k^*)$ correlation function can be expressed as

$$C_{\text{exp}}(k^*) = C_{\text{baseline}}(k^*) \cdot C_{\text{femto}}(k^*), \quad (2)$$

where $C_{\text{baseline}}(k^*)$ describes the non-femtoscopic background which accounts for any residual contributions in $C_{\text{exp}}(k^*)$. In this study, the background in the femtoscopic region primarily arises from elliptic flow [58], which is a consequence of the event-wise angular distribution of particles. The handling of it in the analysis depends on the fitting method and is described in the corresponding sections of the p – p and p – d studies in the text below.

Table 2: The p_T -weighted averages of the PID purity \mathcal{P}_{PID} , the primary fraction $\mathcal{F}_{\text{primary}}$, feed-down contribution of weak decays $\mathcal{F}_{\text{feed-down}}$, and material budget $\mathcal{F}_{\text{material}}$ for (anti)protons and (anti)deuterons. The values are presented as left- and right-range values, corresponding to the 0–10% and 30–50% centrality intervals, respectively.

	$p(\bar{p})$	d	\bar{d}
\mathcal{P}_{PID}	97–99%	93–98%	93–98%
$\mathcal{F}_{\text{primary}}$	88–90%	74–89%	100%
$\mathcal{F}_{\text{feed-down}}$	12–10%	—	—
$\mathcal{F}_{\text{material}}$	< 1%	26–11%	—

The model correlation function accounts not only for the genuine correlations originating from pairs produced in primary processes after collisions, but also for the distortion of the measured correlation function due to particle misidentification and for secondary particles resulting from weak decays and spallation processes in the detector material. These contributions are taken into account by calculating the model correlation function $C_{\text{femto}}(k^*)$ as

$$C_{\text{femto}}(k^*) = 1 + \lambda_{\text{gen}} (C_{\text{gen}}(k^*) - 1) + \lambda_{\text{feed}} (C_{\text{feed}}(k^*) - 1) + \lambda_{\text{misid}} (C_{\text{misid}}(k^*) - 1), \quad (3)$$

which takes into account all contributions with the method discussed in Ref. [40]. In particular, the contributions of genuine and non-genuine particles are quantified by the so-called λ parameters, which can be evaluated as

$$\lambda = \mathcal{P}_i \mathcal{F}_i \mathcal{P}_j \mathcal{F}_j. \quad (4)$$

In this formula, \mathcal{P} represents the PID purity of a given particle species accepted for the study, and \mathcal{F} denotes the fraction of particles of interest with either primary or secondary origin. Both quantities are obtained separately for the two particles contributing to the pair, denoted by the subscripts i, j . The fractions are calculated using approaches already employed in other femtoscopy studies [57, 59]. The identification purity of the (anti)proton is estimated from Monte Carlo (MC) simulations using the HIJING [60] event generator coupled with the GEANT3 [61] transport code. The fraction of correctly identified and misidentified particles within an accepted sample of (anti)deuterons is calculated using a data-driven approach that incorporates information on signals in the TPC and TOF detectors. To estimate the primary and secondary contributions to the (anti)proton samples, a combined MC and data-driven method involving template fits to the DCA_{xy} distributions has been employed. The primary fraction of antideuterons, \mathcal{F} , is assumed to be 100%, as such particles cannot be produced via material knock-out due to baryon number conservation. The average \mathcal{P} and \mathcal{F} fractions for (anti)protons and (anti)deuterons are listed in Tab. 2. Consequently, the genuine component fraction of $C_{\text{femto}}(k^*)$ for correctly identified primary particle pairs corresponds to λ_{gen} , the residual contribution from feed-down of weak decays corresponds to λ_{feed} , and the residual contributions of misidentified particles is given by λ_{misid} . The functional form of C_{gen} is obtained from the model description of the interaction of the pair under study, C_{misid} is assumed to be flat and C_{feed} is obtained by projecting the contribution of weak decays onto the k^* of the genuine pairs. More details about the λ methodology can be found in Refs. [46, 62]. To better reflect the properties of the data samples, the genuine λ_{gen} parameters of p–p and p–d pairs are computed as a function of m_T and k^* , respectively. After applying the λ corrections, no systematic difference is observed between particle and antiparticle pairs within the uncertainties. Since no difference is expected in their interactions, the distributions of particle and antiparticle pairs are combined to reduce the statistical uncertainty. Therefore, in the following text, the terms p–p and p–d refer to the combination of p–p \oplus \bar{p} – \bar{p} and p–d \oplus \bar{p} – \bar{d} , respectively.

From the theoretical perspective, the two-particle correlation function is defined via the Koonin–Pratt formula [29, 63]:

$$C(k^*) = \int S(\mathbf{r}^*) |\psi(\mathbf{r}^*, \mathbf{k}^*)|^2 d^3 r^*, \quad (5)$$

where \mathbf{r}^* describes the relative distance between the two particles in the pair rest frame and $\psi(\mathbf{r}^*, \mathbf{k}^*)$ is the two-particle wave function. The source function $S(\mathbf{r}^*)$ is related to the probability of producing two particles at a relative distance r^* , and it can be modeled using a Gaussian profile:

$$S(\mathbf{r}^*) = \frac{1}{(2\pi R_{ij}^2)^{3/2}} \exp\left(-\frac{r^{*2}}{2R_{ij}^2}\right). \quad (6)$$

Here, the source size, referred to as radius, is characterized by the two-particle Gaussian source width of the distribution of the $i-j$ pair, R_{ij} . In the case of identical particles, $R_{ii} = \sqrt{2}R_i$ where R_i denotes the single-particle femtoscopic source radius. In pp collisions, due to the small source size ($R_i \sim 1.5$ fm), the contributions of short-lived (strongly decaying) resonances ($c\tau \leq 5$ fm) effectively increase the femtoscopic source size by introducing exponential tails to the source function. This effect is known as "resonance halo" [40, 46]. This effect can be neglected for sources of $R_i \sim 3-8$ fm, typical for Pb–Pb collisions, as the convolution of the exponential with a Gaussian does not distort the width of the distribution within the sensitivity of the measurement. Thus, this analysis extracts the effective femtoscopic source radii.

3.1 The proton–proton correlation function and nucleon m_T -scaling

The experimental p–p correlations are investigated and fitted in eight different m_T intervals (1.0–1.3, 1.3–1.4, 1.4–1.5, 1.5–1.6, 1.6–1.7, 1.7–1.8, 1.8–2.0, 2.0–3.2 GeV/ c^2) and three centrality classes using Eqs. (2) and (3). The genuine part of the p–p correlation function, with the contribution λ_{gen} calculated as described for three multiplicity classes mentioned in Sec. 3, is computed employing the CATS [64] framework that includes the Argonne v_{18} (AV18) potential [65], the Coulomb interaction, and the Pauli-blocking effect between the two identical fermions. The $C_{\text{baseline}}(k^*)$ describing the non-femtoscopic background of p–p pairs is modeled using a linear function as a part of the correlation function fit.

To model the experimental p–p correlation function, residual correlations from the feed-down of p– Λ pairs are explicitly considered using Chiral Effective Field Theory at next-to-leading order (χ EFT at NLO) [66–68]. The effect of the p– Λ correlation function on the p–p correlation is included by projecting [40] this contribution onto the k^* of p–p pairs via a decay matrix [69, 70], which is built according to the kinematics of the decay. The contribution from the feed-down of p– Λ pairs to p–p pairs is at most 2%. All other feed-down and misidentification contributions are considered to be flat. All contributions in $C_{\text{femto}}(k^*)$ are smeared to account for the finite momentum resolution of the ALICE detector [69].

The measured p–p correlation function employed to extract the m_T -scaling of R_p is shown in Fig. 1 for one representative m_T interval. The vertical bars and grey boxes represent the statistical and systematic uncertainties of the data, respectively. The systematic uncertainties of the p–p correlation function data points are calculated by varying event and track selection criteria. This includes changing the distance of the primary vertex to the center of the ALICE detector in the beam direction from ± 10 cm to ± 7 cm, the PID selection from 3σ to 2.5σ or 3.5σ , $|\eta|$ range from 0.8 to 0.77 and 0.83, the minimal p_T range from 0.7 GeV/ c to 0.6 or 0.8 GeV/ c , and the number of TPC space points required in the reconstruction process of the tracks from 80 to 70 or 90. The final uncertainty is estimated as the difference between the maximum and minimum values of the correlation function divided by the standard deviation of the uniform distribution. The fitted $C_{\text{exp}}(k^*)$ functions are shown in Fig. 1 by the red bands and the obtained baseline contributions $C_{\text{baseline}}(k^*)$ are shown as light cyan bands. The resulting baseline shows no significant contribution to the correlation function. The transition from central to peripheral collisions

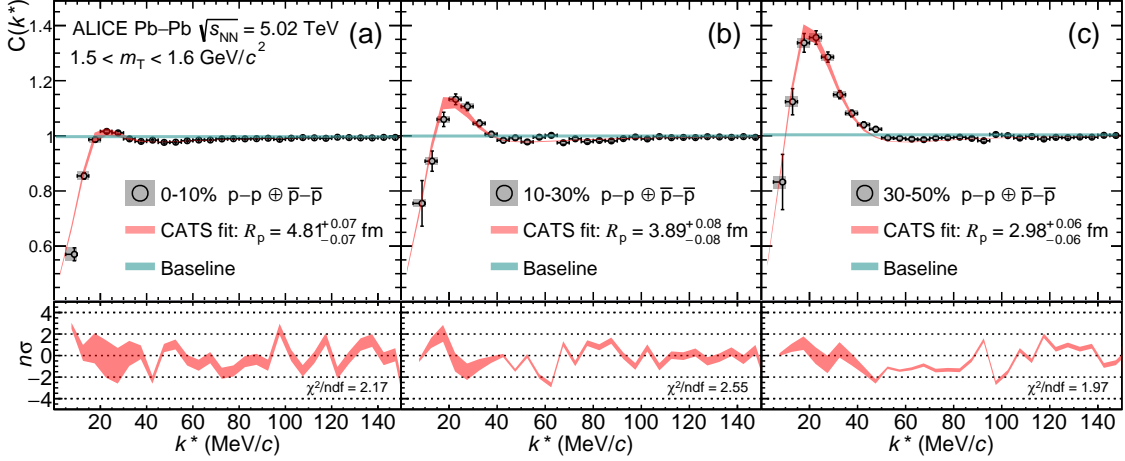


Figure 1: Top panels: raw p-p correlation functions as a function of k^* in one exemplary m_T interval obtained from Pb–Pb collisions at $\sqrt{s_{\text{NN}}} = 5.02$ TeV in the 0–10% (a), 10–30% (b) and 30–50% (c) centrality intervals, respectively. The black open markers represent the data, while the vertical lines and the boxes indicate the statistical and systematic uncertainties, respectively. The red region represents the 1σ uncertainty range of the fits performed using CATS [64]. The non-femtoscopic background contributions are shown by the light cyan bands. Bottom panels: n_σ calculated as data-to-fit difference, normalized by the total uncertainty of experimental data.

in a given m_T interval leads to a smaller emission source size, which visibly impacts the strength of the correlation function. This behavior is accurately captured by the fitting procedure currently employed.

The R_p values obtained from fitting the p-p correlation function across each m_T interval are displayed in the left panel of Fig. 2. These values are shown for the 0–10%, 10–30%, and 30–50% centrality intervals, represented by solid red, blue, and green markers, respectively. The measured femtoscopic source sizes are relatively large, ranging from a minimum of $2.73^{+0.05}_{-0.05}$ fm for the highest m_T bin in the 30–50% centrality collisions to $5.66^{+0.16}_{-0.16}$ fm for the lowest m_T bin in the 0–10% centrality collisions. The values are quoted with combined systematic and statistical uncertainties. The systematic uncertainties of all R_p are estimated as 1σ of the source radii distribution calculated for different settings of the analysis and fitting method. The uncertainties contributing from the experimental correlation functions are accounted by the bootstrap method [71] where data points are resampled using a Gaussian distribution of the statistical and systematic error. The uncertainty originating from the fitting technique is taken into account by modifying the upper limit of the fit region 300 ± 50 MeV/c, employing the baseline considered as a polynomial of the first or third degree with a fixed linear term, and modifying the λ_{gen} parameters by up to $\pm 5\%$, addressing potential underestimation or overestimation of these settings. Shaded bands in the left panel represent the 1σ uncertainties of the femtoscopic source sizes dependence of m_T , described using a power-law parametrization, $R_p = a + b \cdot \langle m_T \rangle^c$. The obtained values of the parameters a, b, c are summarized in Appendix A. The values of R_p exhibit the same trend with increasing m_T observed in previous femtoscopy analyses of π , K, and p in Pb–Pb collisions at $\sqrt{s_{\text{NN}}} = 2.76$ TeV [35]. The m_T scaling presented in the figure also includes nucleon-systems measurements from a proton-deuteron study, based on three-body (denoted in the figure as PISA) and two-body (L–L) analyses, which are described in more detail in the next section. Furthermore, the measured R_p grows linearly with the cube root of the charged particle multiplicity for all m_T ranges separately, as shown in the right panel of Fig. 2. The bands of this panel depict 1σ uncertainties of fits to the $\langle dN_{\text{ch}}/d\eta \rangle^{1/3}$ dependence of R_p , obtained using $R_p = A \cdot \langle dN_{\text{ch}}/d\eta \rangle^{1/3} + B$. The obtained values of the parameters A, B are summarized in Appendix A.

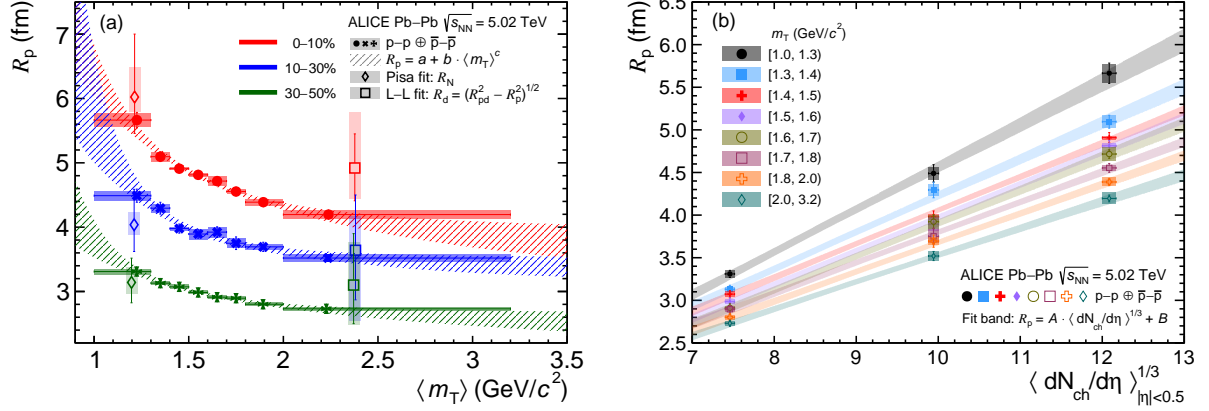


Figure 2: Left panel: The femtoscopic source size of protons (R_p) measured as a function of m_T in Pb–Pb collisions at $\sqrt{s_{NN}} = 5.02$ TeV is represented by full red, blue, and green markers for the 0–10%, 10–30%, 30–50% centrality intervals, respectively. The open diamond and squared markers represent the values of femtoscopic source sizes of nucleons (R_N) and deuterons (R_d), obtained by fitting the measured p–d correlation function with the L–L [48] and Pisa [49] models, where in the later the AV18 [65]+UIX [72] potential is used. Right panel: R_p as a function of $\langle dN_{ch}/d\eta \rangle^{1/3}$ for eight m_T intervals. The shaded bands in the two panels depict the m_T and $\langle dN_{ch}/d\eta \rangle^{1/3}$ dependence of the measured radii fitted with power-law function, $R_p = a + b \cdot \langle m_T \rangle^c$, and linear function $R_p = A \cdot \langle dN_{ch}/d\eta \rangle^{1/3} + B$, respectively. The bandwidth reflects the 1σ range of the fit solutions, obtained by bootstrapping the radii over their statistical and systematic uncertainties.

3.2 The proton–deuteron correlation function

The genuine p–d correlation functions for the three centrality intervals considered in this study are presented in Fig. 3. A flat distribution is assumed for the p–d pairs originating from any of the secondary processes listed in Eq. (3). Therefore, the genuine p–d functions are constrained based on experimental measurements as $C_{gen}(k^*) = (C_{femto}(k^*) - 1)/\lambda_{gen} + 1$. The baseline presented in Fig. 3 as a light cyan line is obtained when considering the event-wise particle correlations due to elliptic flow, which contributes to the femtoscopic range of the p–d correlations in heavy-ion collisions. The single-particle azimuthal anisotropies result in a two-particle correlation in relative momentum space, which can be calculated using a data-driven approach. The calculation uses a Monte Carlo data resampling method using measured elliptic flow coefficients [23, 73] and momentum distributions of the considered particles. The obtained distribution was normalized by the one obtained using the same momenta distributions but with a flat azimuthal anisotropy. The resulting baseline shows no significant contribution to the correlation function. The vertical bars and gray boxes of the data points represent the statistical and systematic uncertainties, respectively. The systematic uncertainties of the p–d correlation functions data points are estimated based on variations of the analysis settings such as the selection of events and particles described in Sec. 2, following the same pattern of settings and methodology as in Ref. [74].

In order to extract the source size of the p–d system, the genuine p–d correlation function is first calculated using the method developed by the Pisa group [49]. This method employs a complete three-body treatment of the p–d system within the Hyperspherical Harmonics (HH) approach [75, 76] and accounts for strong interactions in p–d by using the AV18 potential [65] for two-nucleon (NN) and the Urbana IX (UIX) potential [72] for three-nucleon (NNN) interactions, as well as the Coulomb potential for both the short- and asymptotic-range interactions. In the full calculations, all the partial waves up to $J^\pi = \frac{7}{2}^-$ are included providing an excellent description of the p–d correlation function in pp collisions [59]. In the following, the full three-body calculations are referred to as AV18+UIX calculations. Since the AV18+UIX calculations employ nucleons as the degrees of freedom, the relevant source term in this approach is derived under the condition that each nucleon in the three-body system is characterized by

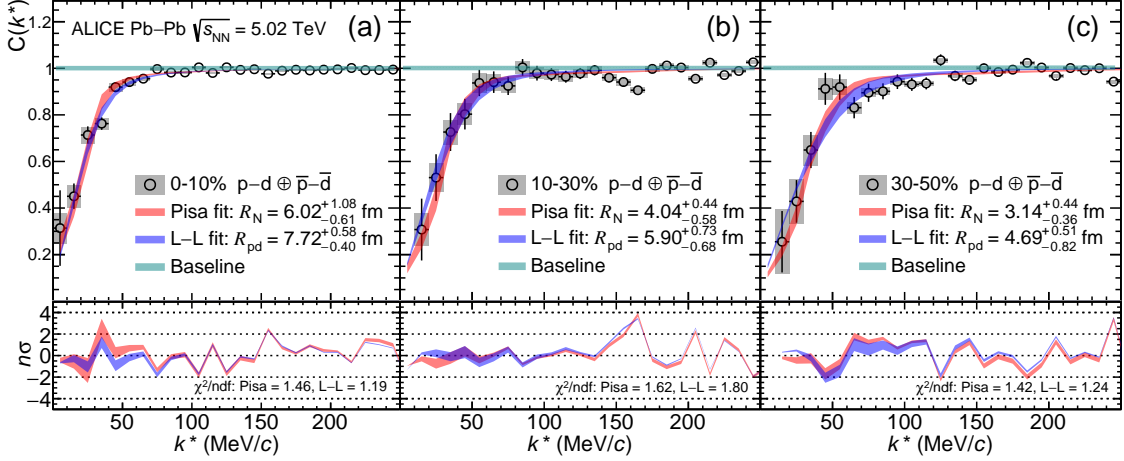


Figure 3: Top panels: genuine p-d correlation function as a function of k^* obtained from Pb–Pb collisions at $\sqrt{s_{\text{NN}}} = 5.02$ TeV in the 0–10% (a), 10–30% (b) and 30–50% (c) centrality intervals, respectively. The measured data are shown as black open markers, while the vertical lines and the boxes represent the statistical and systematic uncertainties, respectively. The correlation functions are shown together with a fit band of 1σ uncertainties performed using the three-body approach employing AV18+UIX potentials (Pisa fit, red bands) and using the Lednický–Lyuboshitz approach (L–L fit, blue bands). The non-femtoscopic background contributions are represented by the light cyan band. Bottom panels: n_σ calculated as data-to-fit difference, normalized by the total uncertainty of experimental data.

the same femtoscopic source radius of the nucleon–nucleon pair, R_N . The source size R_N is extracted across the three centrality intervals, from the measured p-d correlations employing the χ^2 minimization method [35, 57] on the theoretical correlation functions given by a full three-body approach. The values of the source size parameter R_N are $6.02^{+1.08}_{-0.61}$, $4.04^{+0.44}_{-0.58}$, and $3.14^{+0.44}_{-0.36}$ fm for the 0–10%, 10–30%, and 30–50% centrality intervals, respectively. The modeled correlation function exhibits an excellent agreement with the measured correlation function for all three centrality intervals, as demonstrated in the upper panels of Fig. 3. Since the NN pairs contribute to forming the p-(p-n) system [59] at small k^* , it is reasonable to evenly distribute the total momentum $2k_T$ of the p-d pair into the three nucleons. Based on the above definition, the m_T of a nucleon inside the p-d system can be written as $m_T = \sqrt{\left(2k_T^{pd}/3\right)^2 + m_p^2}$ and is found to be approximately 1.2 GeV/ c^2 . The R_N parameters measured in this study are shown as empty diamond markers in Fig. 2. The values of the parameters are in agreement with the proton m_T -scaling measured above. This consistency confirms the validity of the m_T -scaling for nucleon pairs that form a p-d system.

Traditionally, the genuine p-d correlation functions can also be modeled using the Lednický–Lyuboshitz (L–L) formalism [48], which assumes two point-like particles. In this method, the deuteron is treated as a single particle rather than the two nucleons being considered individually in the final interaction, which requires scattering parameters as input. In this study, these parameters are taken from five different theoretical analyses of p-d scattering data [77–81]. In addition, the source size of the p-d system in the L–L method is determined based on the non-identical pair source expression $R_{ij} = \sqrt{R_i^2 + R_j^2}$ [45]. Here, $R_{i/j}$ denotes the single particle femtoscopic source size of a proton and a deuteron for corresponding m_T of particles that contribute to the p-d k^* range (0, 250) MeV/ c . In this range, the experimental p-d correlations are fitted using the L–L model with R_{pd} as a free parameter by employing the χ^2 minimization method. An example of fitting results using representative scattering parameters [78] is shown as a blue band in Fig. 3. Similarly to the three-body case, the two-body L–L approach also shows good agreement with the experimental data, unlike the p-d measurement in pp collisions [59]. The L–L model used for pp collision data with small femtoscopic sources predicts an unphysical peak at very small k^* ,

which is not observed in any data. Removing this artifact requires applying detailed inner corrections or exact solutions of the scattering problem, which accounts for the detailed dynamics of the p–d pair. In large systems, such as those in heavy-ion collisions, the average intermediate distances between the considered particles are larger, making the results less sensitive to potential discrepancies caused by approximate solutions in the inner system region [82].

Furthermore, the deuteron source size is extracted using the expression $R_d = \sqrt{R_{pd}^2 - R_p^2}$, where R_p is the single particle femtoscopic source size for the proton, constrained by m_T -scaling of p–p pairs shown in Fig. 2. The R_d values are evaluated taking an average of the results obtained by fitting the L–L model with the five different scattering parameters [77–81] for the strong interaction. The values of R_d are $4.92^{+1.02}_{-0.69}$, $3.64^{+1.01}_{-1.33}$, and $3.10^{+1.04}_{-0.86}$ fm for the 0–10%, 10–30%, and 30–50% centrality intervals, respectively. The measured femtoscopic source sizes of deuterons are represented in Fig. 2 by the square markers, corresponding to the m_T of deuterons contributing to low k^* values, which is approximately $2.4 \text{ GeV}/c^2$ for the three centrality intervals.

The extracted single particle source sizes for deuterons are in agreement with m_T -scaling for p–p pairs, suggesting that deuterons, as composite light nuclei, share a common flow velocity with nucleons in Pb–Pb collisions. The observations based on radial and elliptic flow [23] bear different natures, thus conclusions from one cannot be directly extrapolated to the other. This is because elliptic flow and femtoscopic studies measure the system in different spaces. Therefore, in femtoscopic correlation functions, the effect of elliptic flow is a long-range background beneath the FSI signal. On the other hand, the radial flow directly affects the source function, thus the measured radii. The single deuteron radii have been previously obtained with larger systematic uncertainties of approximately 50% in a study of pion-deuteron correlation functions [74], originating mainly from the imprecise data used to estimate the pion component in the pion-deuteron source. The radii measured in the two studies are consistent with the combined statistical and systematic uncertainties.

The uncertainties of the femtoscopic radii measured in the p–d study are shown in Fig. 3 with combined statistical and systematic uncertainties. They are derived from the 1σ range of the distribution of source sizes obtained by resampling the data points of the correlation functions within their systematic and statistical uncertainties, as well as by varying the fitting settings, which include: the upper limit of the fit region 150 or 250 MeV/ c , modification of the λ_{gen} factor by $\pm 5\%$, and the baseline obtained from the simulation of the elliptic flow effect or second-order polynomial fit to the normalization region. In addition, R_d accounts for the uncertainty originating from the R_p source prediction by resampling R_p using bootstrap over its uncertainties, as well as from the scattering parameters used in the L–L parameterization.

The radii extracted for different m_T values within the same centrality classes for the p–d system are currently compatible within uncertainties for two- and three-body methods. However, more precise measurements could enable us to test m_T -scaling for p–d pairs with a level of precision comparable to that already achieved for p–p pairs. The ongoing Run 3 at the LHC, where the ALICE detector has been upgraded to handle a rate 100 times larger than that of the Run 2 campaigns, will facilitate these precise measurements [83].

The correlation functions shown in Fig. 3 demonstrate the repulsive nature of p–d interactions in heavy-ion collisions, which can be accurately described only by including FSI in the model. The experimentally observed presence of FSI between the analyzed particles in Pb–Pb collisions, along with the complementary study of p–p collisions [59], supports further the notion of an early deuteron formation, as demonstrated in Ref. [84] and theoretically stated in Ref. [85].

The fact that both two- and three-body calculations provide an excellent description of the experimental data and that the obtained R_N and R_d radii values match the nucleon m_T -scaling independently measured for p–p pairs demonstrates the sensitivity of the femtoscopy method, applied to ALICE data for differ-

ent colliding systems, to the detailed features of the strong interaction. Indeed, the previous analysis conducted for pp collisions at 13 TeV demonstrated that the two-body approach fails at small distances due to the short-range features of the interaction, which cannot be adequately described by two-body calculations with the L–L model [59]. However, the three-body calculation provides the same description of the p–d data as the two-body calculation in Pb–Pb collisions where the inter-particle distances are sufficiently large so that the short-range nature of the interaction no longer affects the correlation observable.

Furthermore, in the two-body case, the obtained radii correspond to the m_T of the deuteron treated as a nucleon-based composite particle, whereas in the three-body case, the measured radii reflect the femtoscopic size of nucleons forming the deuteron at the m_T of a single nucleon. The fact that the radii of the deuteron and the nucleon align with the general m_T -scaling trend highlights that the nucleons forming deuterons cannot be distinguished from other nucleons based on this scaling.

4 Summary

In conclusion, this work presents the first detailed study of p–p and p–d correlation functions measured in Pb–Pb collisions at $\sqrt{s_{NN}} = 5.02$ TeV by ALICE at the LHC by employing state-of-the-art interaction models. The m_T -scaling of proton femtoscopic source radii has been measured for three centrality classes in Pb–Pb collisions, and both two- and three-body calculations have been employed to describe the p–d correlation functions successfully. This agreement demonstrates that in Pb–Pb collisions, the three-body approach converges to the two-body ones because of the increasing inter-particle distances. The nucleon femtoscopic source radii obtained from the fits range from $2.73^{+0.05}_{-0.05}$ fm in 30–50% centrality collisions to $5.66^{+0.16}_{-0.16}$ fm in 0–10% centrality collisions, quantitatively supporting this conclusion. Moreover, the source values obtained from the two- and three-body fits follow the m_T -scaling of the proton source radii, supporting the hypothesis that the deuteron, as a nucleon-based composite object, shares common flow velocities with protons. Since uncertainties are still sizable, more experimental data, particularly from the upcoming Run 3 measurement, will be crucial to verify this hypothesis and improve the precision of these results.

Acknowledgements

The ALICE Collaboration would like to thank all its engineers and technicians for their invaluable contributions to the construction of the experiment and the CERN accelerator teams for the outstanding performance of the LHC complex. The ALICE Collaboration gratefully acknowledges the resources and support provided by all Grid centres and the Worldwide LHC Computing Grid (WLCG) collaboration. The ALICE Collaboration acknowledges the following funding agencies for their support in building and running the ALICE detector: A. I. Alikhanyan National Science Laboratory (Yerevan Physics Institute) Foundation (ANSL), State Committee of Science and World Federation of Scientists (WFS), Armenia; Austrian Academy of Sciences, Austrian Science Fund (FWF): [M 2467-N36] and Nationalstiftung für Forschung, Technologie und Entwicklung, Austria; Ministry of Communications and High Technologies, National Nuclear Research Center, Azerbaijan; Conselho Nacional de Desenvolvimento Científico e Tecnológico (CNPq), Financiadora de Estudos e Projetos (Finep), Fundação de Amparo à Pesquisa do Estado de São Paulo (FAPESP) and The Sao Paulo Research Foundation (FAPESP), Brazil; Bulgarian Ministry of Education and Science, within the National Roadmap for Research Infrastructures 2020–2027 (object CERN), Bulgaria; Ministry of Education of China (MOEC), Ministry of Science & Technology of China (MSTC) and National Natural Science Foundation of China (NSFC), China; Ministry of Science and Education and Croatian Science Foundation, Croatia; Centro de Aplicaciones Tecnológicas y Desarrollo Nuclear (CEADEN), Cubaenergía, Cuba; Ministry of Education, Youth and Sports of the Czech Republic, Czech Republic; The Danish Council for Independent Research | Natural Sciences, the

VILLUM FONDEN and Danish National Research Foundation (DNRF), Denmark; Helsinki Institute of Physics (HIP), Finland; Commissariat à l’Energie Atomique (CEA) and Institut National de Physique Nucléaire et de Physique des Particules (IN2P3) and Centre National de la Recherche Scientifique (CNRS), France; Bundesministerium für Bildung und Forschung (BMBF) and GSI Helmholtzzentrum für Schwerionenforschung GmbH, Germany; General Secretariat for Research and Technology, Ministry of Education, Research and Religions, Greece; National Research, Development and Innovation Office, Hungary; Department of Atomic Energy Government of India (DAE), Department of Science and Technology, Government of India (DST), University Grants Commission, Government of India (UGC) and Council of Scientific and Industrial Research (CSIR), India; National Research and Innovation Agency - BRIN, Indonesia; Istituto Nazionale di Fisica Nucleare (INFN), Italy; Japanese Ministry of Education, Culture, Sports, Science and Technology (MEXT) and Japan Society for the Promotion of Science (JSPS) KAKENHI, Japan; Consejo Nacional de Ciencia (CONACYT) y Tecnología, through Fondo de Cooperación Internacional en Ciencia y Tecnología (FONCICYT) and Dirección General de Asuntos del Personal Académico (DGAPA), Mexico; Nederlandse Organisatie voor Wetenschappelijk Onderzoek (NWO), Netherlands; The Research Council of Norway, Norway; Pontificia Universidad Católica del Perú, Peru; Ministry of Science and Higher Education, National Science Centre and WUT ID-UB, Poland; Korea Institute of Science and Technology Information and National Research Foundation of Korea (NRF), Republic of Korea; Ministry of Education and Scientific Research, Institute of Atomic Physics, Ministry of Research and Innovation and Institute of Atomic Physics and Universitatea Națională de Știință și Tehnologie Politehnica Bucuresti, Romania; Ministerstvo školstva, výskumu, vývoja a mládeže SR, Slovakia; National Research Foundation of South Africa, South Africa; Swedish Research Council (VR) and Knut & Alice Wallenberg Foundation (KAW), Sweden; European Organization for Nuclear Research, Switzerland; Suranaree University of Technology (SUT), National Science and Technology Development Agency (NSTDA) and National Science, Research and Innovation Fund (NSRF via PMU-B B05F650021), Thailand; Turkish Energy, Nuclear and Mineral Research Agency (TENMAK), Turkey; National Academy of Sciences of Ukraine, Ukraine; Science and Technology Facilities Council (STFC), United Kingdom; National Science Foundation of the United States of America (NSF) and United States Department of Energy, Office of Nuclear Physics (DOE NP), United States of America. In addition, individual groups or members have received support from: Czech Science Foundation (grant no. 23-07499S), Czech Republic; FORTE project, reg. no. CZ.02.01.01/00/22_008/0004632, Czech Republic, co-funded by the European Union, Czech Republic; European Research Council (grant no. 950692), European Union; Deutsche Forschungs Gemeinschaft (DFG, German Research Foundation) “Neutrinos and Dark Matter in Astro- and Particle Physics” (grant no. SFB 1258), Germany; ICSC - National Research Center for High Performance Computing, Big Data and Quantum Computing and FAIR - Future Artificial Intelligence Research, funded by the NextGenerationEU program (Italy).

References

- [1] N. Cabibbo and G. Parisi, “Exponential hadronic spectrum and quark liberation”, *Phys. Lett. B* **59** (1975) 67–69.
- [2] E. V. Shuryak, “Quantum chromodynamics and the theory of superdense matter”, *Phys. Rep.* **61** (1980) 71–158.
- [3] U. W. Heinz and M. Jacob, “Evidence for a new state of matter: An Assessment of the results from the CERN lead beam program”, [arXiv:nucl-th/0002042](https://arxiv.org/abs/nucl-th/0002042).
- [4] **BRAHMS** Collaboration, I. Arsene *et al.*, “Quark gluon plasma and color glass condensate at RHIC? The Perspective from the BRAHMS experiment”, *Nucl. Phys. A* **757** (2005) 1–27, [arXiv:nucl-ex/0410020](https://arxiv.org/abs/nucl-ex/0410020).

- [5] **PHOBOS** Collaboration, B. B. Back *et al.*, “The PHOBOS perspective on discoveries at RHIC”, *Nucl. Phys. A* **757** (2005) 28–101, arXiv:nucl-ex/0410022.
- [6] **STAR** Collaboration, J. Adams *et al.*, “Experimental and theoretical challenges in the search for the quark gluon plasma: The STAR Collaboration’s critical assessment of the evidence from RHIC collisions”, *Nucl. Phys. A* **757** (2005) 102–183, arXiv:nucl-ex/0501009.
- [7] **PHENIX** Collaboration, K. Adcox *et al.*, “Formation of dense partonic matter in relativistic nucleus–nucleus collisions at RHIC: experimental evaluation by the PHENIX collaboration”, *Nucl. Phys. A* **757** (2005) 184–283, arXiv:nucl-ex/0410003.
- [8] **ALICE** Collaboration, Acharya, Shreyasi and others, “The ALICE experiment: a journey through QCD”, *Eur. Phys. J. C* **84** (2024) 813, arXiv:2211.04384 [nucl-ex].
- [9] S. A. Bass, A. Dumitru, M. Bleicher, L. Bravina, E. Zabrodin, H. Stoecker, and W. Greiner, “Hadronic freezeout following a first order hadronization phase transition in ultrarelativistic heavy ion collisions”, *Phys. Rev. C* **60** (1999) 021902, arXiv:nucl-th/9902062.
- [10] M. Bleicher and J. Aichelin, “Strange resonance production: Probing chemical and thermal freezeout in relativistic heavy ion collisions”, *Phys. Lett. B* **530** (2002) 81–87, arXiv:hep-ph/0201123.
- [11] J. Letessier and J. Rafelski, *Hadrons and Quark–Gluon Plasma*. Cambridge Monographs on Particle Physics, Nuclear Physics and Cosmology. 2002.
- [12] V. Vovchenko and H. Stoecker, “Thermal-FIST: A package for heavy-ion collisions and hadronic equation of state”, *Comput. Phys. Commun.* **244** (2019) 295–310, arXiv:1901.05249 [nucl-th].
- [13] **ALICE** Collaboration, S. Acharya *et al.*, “Production of ${}^4\text{He}$ and ${}^4\overline{\text{He}}$ in Pb–Pb collisions at $\sqrt{s_{\text{NN}}} = 2.76$ TeV at the LHC”, *Nucl. Phys. A* **971** (2018) 1–20, arXiv:1710.07531 [nucl-ex].
- [14] A. Andronic, P. Braun-Munzinger, K. Redlich, and J. Stachel, “Decoding the phase structure of QCD via particle production at high energy”, *Nat.* **561** (2018) 321–330, arXiv:1710.09425 [nucl-th].
- [15] T. Hatsuda, “Lattice quantum chromodynamics and baryon-baryon interactions”, *Front. Phys.* **13** (2018) 1–10.
- [16] C. Van Der Leun and C. Alderliesten, “The deuteron binding energy”, *Nucl. Phys. A* **380** (1982) 261–269.
- [17] R. Scheibl and U. W. Heinz, “Coalescence and flow in ultrarelativistic heavy ion collisions”, *Phys. Rev. C* **59** (1999) 1585–1602, arXiv:nucl-th/9809092.
- [18] K.-J. Sun, R. Wang, C. M. Ko, Y.-G. Ma, and C. Shen, “Unveiling the dynamics of little-bang nucleosynthesis”, *Nat. Commun.* **15** (2024) 1074, arXiv:2207.12532 [nucl-th].
- [19] **ALICE** Collaboration, J. Adam *et al.*, “Production of light nuclei and anti-nuclei in pp and Pb–Pb collisions at energies available at the CERN Large Hadron Collider”, *Phys. Rev. C* **93** (2016) 024917, arXiv:1506.08951 [nucl-ex].
- [20] **ALICE** Collaboration, S. Acharya *et al.*, “Measurement of deuteron spectra and elliptic flow in Pb–Pb collisions at $\sqrt{s_{\text{NN}}} = 2.76$ TeV at the LHC”, *Eur. Phys. J. C* **77** (2017) 658, arXiv:1707.0730 [nucl-ex].

- [21] S. A. Voloshin, A. M. Poskanzer, and R. Snellings, “Collective Phenomena in Non-Central Nuclear Collisions”, *Landolt-Bornstein* **23** (2010) 293–333, arXiv:0809.2949 [nucl-ex].
- [22] **STAR** Collaboration, L. Adamczyk *et al.*, “Measurement of elliptic flow of light nuclei at $\sqrt{s_{NN}} = 200, 62.4, 39, 27, 19.6, 11.5$, and 7.7 GeV at the BNL Relativistic Heavy Ion Collider”, *Phys. Rev. C* **94** (2016) 034908, arXiv:1601.07052 [nucl-ex].
- [23] **ALICE** Collaboration, S. Acharya *et al.*, “Elliptic and triangular flow of (anti)deuterons in Pb–Pb collisions at $\sqrt{s_{NN}} = 5.02$ TeV”, *Phys. Rev. C* **102** (2020) 055203, arXiv:2005.14639 [nucl-ex].
- [24] **ALICE** Collaboration, S. Acharya *et al.*, “First Measurement of Antideuteron Number Fluctuations at Energies Available at the Large Hadron Collider”, *Phys. Rev. Lett.* **131** (2023) 041901, arXiv:2204.10166 [nucl-ex].
- [25] M. Kachelrieß, S. Ostapchenko, and J. Tjemmland, “Alternative coalescence model for deuteron, tritium, helium-3 and their antinuclei”, *Eur. Phys. J. A* **56** (2020) 4, arXiv:1905.01192 [hep-ph].
- [26] K. Blum and M. Takimoto, “Nuclear coalescence from correlation functions”, *Phys. Rev. C* **99** (2019) 044913, arXiv:1901.07088 [nucl-th].
- [27] M. Mahlein, L. Barioglio, F. Bellini, L. Fabbietti, C. Pinto, B. Singh, and S. Tripathy, “A realistic coalescence model for deuteron production”, *Eur. Phys. J. C* **83** (2023) 804, arXiv:2302.12696 [hep-ex].
- [28] S. Mrówczyński and P. Słoń, “Hadron–deuteron correlations and production of light nuclei in relativistic heavy-ion collisions”, *Acta Phys. Polon. B* **51** (2020) 1739–1755, arXiv:1904.08320 [nucl-th].
- [29] M. A. Lisa, S. Pratt, R. Soltz, and U. Wiedemann, “Femtoscopy in relativistic heavy ion collisions: Two decades of progress”, *Ann. Rev. Nucl. Part. Sci.* **55** (2005) 357–402, arXiv:nucl-ex/0505014 [nucl-ex].
- [30] **ALICE** Collaboration, K. Aamodt *et al.*, “Femtoscopy of pp collisions at $\sqrt{s} = 0.9$ and 7 TeV at the LHC with two-pion Bose-Einstein correlations”, *Phys. Rev. D* **84** (2011) 112004, arXiv:1101.3665 [nucl-ex].
- [31] **ALICE** Collaboration, K. Aamodt *et al.*, “Two-pion Bose-Einstein correlations in pp collisions at $\sqrt{s} = 900$ GeV”, *Phys. Rev. D* **82** (2010) 052001, arXiv:1007.0516 [nucl-ex].
- [32] **ALICE** Collaboration, J. Adam *et al.*, “Two-pion femtoscopy in p–Pb collisions at $\sqrt{s_{NN}} = 5.02$ TeV”, *Phys. Rev. C* **91** (2015) 034906, arXiv:1502.00559 [nucl-ex].
- [33] **ALICE** Collaboration, J. Adam *et al.*, “Centrality dependence of pion freeze-out radii in Pb–Pb collisions at $\sqrt{s_{NN}} = 2.76$ TeV”, *Phys. Rev. C* **93** (2016) 024905, arXiv:1507.06842 [nucl-ex].
- [34] **ALICE** Collaboration, S. Acharya *et al.*, “Pion-kaon femtoscopy and the lifetime of the hadronic phase in Pb–Pb collisions at $\sqrt{s_{NN}} = 2.76$ TeV”, *Phys. Lett. B* **813** (2021) 136030, arXiv:2007.08315 [nucl-ex].
- [35] **ALICE** Collaboration, J. Adam *et al.*, “One-dimensional pion, kaon, and proton femtoscopy in Pb–Pb collisions at $\sqrt{s_{NN}} = 2.76$ TeV”, *Phys. Rev. C* **92** (2015) 054908, arXiv:1506.07884 [nucl-ex].

- [36] **STAR** Collaboration, C. Adler *et al.*, “Pion interferometry of $\sqrt{s_{\text{NN}}} = 130$ GeV Au+Au collisions at RHIC”, *Phys. Rev. Lett.* **87** (2001) 082301, arXiv:nucl-ex/0107008 [nucl-ex].
- [37] **PHENIX** Collaboration, S. S. Adler *et al.*, “Bose-Einstein Correlations of Charged Pion Pairs in Au + Au Collisions at $\sqrt{s_{\text{NN}}} = 200$ GeV”, *Phys. Rev. Lett.* **93** (2004) 152302, arXiv:nucl-ex/0401003 [nucl-ex].
- [38] **STAR** Collaboration, B. I. Abelev *et al.*, “Pion interferometry in Au+Au and Cu+Cu collisions at $\sqrt{s_{\text{NN}}} = 62.4$ and 200 GeV”, *Phys. Rev. C* **80** (2009) 024905, arXiv:0903.1296 [nucl-ex].
- [39] **ALICE** Collaboration, K. Aamodt *et al.*, “Two-pion Bose-Einstein correlations in central Pb–Pb collisions at $\sqrt{s_{\text{NN}}} = 2.76$ TeV”, *Phys. Lett. B* **696** (02, 2011) 328–337, arXiv:1012.4035 [nucl-ex].
- [40] **ALICE** Collaboration, S. Acharya *et al.*, “Search for a common baryon source in high-multiplicity pp collisions at the LHC”, *Phys. Lett. B* **811** (2020) 135849, arXiv:2004.08018 [nucl-ex]. [Corrigendum: *Phys. Lett. B* **861** (2025) 139233].
- [41] **STAR** Collaboration, J. Adams *et al.*, “Pion interferometry in Au+Au collisions at $\sqrt{s_{\text{NN}}} = 200$ GeV”, *Phys. Rev. C* **71** (2005) 044906, arXiv:nucl-ex/0411036 [nucl-ex].
- [42] A. Kisiel, M. Gałażyn, and P. Bożek, “Pion, kaon, and proton femtoscopy in Pb–Pb collisions at $\sqrt{s_{\text{NN}}} = 2.76$ TeV modeled in (3+1)D hydrodynamics”, *Phys. Rev. C* **90** (2014) 064914, arXiv:1409.4571 [nucl-th].
- [43] A. Kisiel, “Pion-kaon femtoscopy in Pb–Pb collisions at $\sqrt{s_{\text{NN}}} = 2.76$ TeV modeled in (3+1)D hydrodynamics coupled to Therminator 2 and the effect of delayed kaon emission”, *Phys. Rev. C* **98** (2018) 044909, arXiv:1804.06781 [nucl-th].
- [44] V. M. Shapoval and Yu. M. Sinyukov, “Bulk observables in Pb–Pb collisions at $\sqrt{s_{\text{NN}}} = 5.02$ TeV at the CERN Large Hadron Collider within the integrated hydrookinetic model”, *Phys. Rev. C* **100** (2019) 044905, arXiv:1809.07400 [nucl-ph].
- [45] A. Kisiel, “Nonidentical-particle femtoscopy at $\sqrt{s_{\text{NN}}} = 200$ GeV in hydrodynamics with statistical hadronization”, *Phys. Rev. C* **81** (2010) 064906, arXiv:0909.5349 [nucl-th].
- [46] **ALICE** Collaboration, Acharya, S. and others, “Common femtoscopy hadron-emission source in pp collisions at the LHC”, *Eur. Phys. J. C* **85** (2025) 198, arXiv:2311.14527 [hep-ph].
- [47] **ALICE** Collaboration, S. Acharya *et al.*, “Investigating the p- π^\pm and p-p- π^\pm dynamics with femtoscopy in pp collisions at $\sqrt{s} = 13$ TeV”, arXiv:2502.20200 [nucl-ex].
- [48] R. Lednicky and V. L. Lyuboshits, “Final state interaction effect on pairing correlations between particles with Small Relative Momenta”, *Sov. J. Nucl. Phys.* **35** (1982) 770. [*Yad. Fiz.* **35** (1981) 1316].
- [49] M. Viviani, S. König, A. Kievsky, L. E. Marcucci, B. Singh, and O. Vázquez Doce, “Role of three-body dynamics in nucleon-deuteron correlation functions”, *Phys. Rev. C* **108** (2023) 064002, arXiv:2306.02478 [nucl-th].
- [50] **ALICE** Collaboration, K. Aamodt *et al.*, “The ALICE experiment at the CERN LHC”, *JINST* **3** (2008) S08002.
- [51] **ALICE** Collaboration, B. B. Abelev *et al.*, “Performance of the ALICE Experiment at the CERN LHC”, *Int. J. Mod. Phys. A* **29** (2014) 1430044, arXiv:1402.4476 [nucl-ex].

- [52] ALICE Collaboration, K. Aamodt *et al.*, “Alignment of the ALICE Inner Tracking System with cosmic-ray tracks”, *JINST* **5** (2010) P03003, arXiv:1001.0502 [physics.ins-det].
- [53] ALICE Collaboration, P. Gasik, “Upgrade of the ALICE central barrel tracking detectors: ITS and TPC”, *Nucl. Phys. A* **982** (2019) 943–946, arXiv:1807.07787 [physics.ins-det].
- [54] ALICE Collaboration, E. Abbas *et al.*, “Performance of the ALICE VZERO system”, *JINST* **8** (2013) P10016, arXiv:1306.3130 [nucl-ex].
- [55] ALICE Collaboration, B. Abelev *et al.*, “Centrality determination of Pb–Pb collisions at $\sqrt{s_{\text{NN}}} = 2.76$ TeV with ALICE”, *Phys. Rev. C* **88** (2013) 044909, arXiv:1301.4361 [nucl-ex].
- [56] ALICE Collaboration, “Centrality Determination in Heavy Ion Collisions”, (2018). <https://cds.cern.ch/record/2636623>.
- [57] ALICE Collaboration, S. Acharya and et al, “Kaon–proton strong interaction at low relative momentum via femtoscopy in Pb–Pb collisions at the LHC”, *Phys. Lett. B* **822** (2021) 136708, arXiv:2105.05683 [nucl-ex].
- [58] A. Kisiel, “Non-identical particle correlation analysis in the presence of non-femtoscopic correlations”, *Acta Phys. Polon. B* **48** (2017) 717.
- [59] ALICE Collaboration, S. Acharya *et al.*, “Exploring the Strong Interaction of Three-Body Systems at the LHC”, *Phys. Rev. X* **14** (2024) 031051, arXiv:2308.16120 [nucl-ex].
- [60] X.-N. Wang and M. Gyulassy, “HIJING: A Monte Carlo model for multiple jet production in p-p, p-A and A-A collisions”, *Phys. Rev. D* **44** (1991) 3501–3516.
- [61] R. Brun, F. Bruyant, F. Carminati, S. Giani, M. Maire, A. McPherson, G. Patrick, and L. Urban, *GEANT: Detector Description and Simulation Tool; Oct 1994*. CERN Program Library. CERN, Geneva, 1993. Long Writeup W5013.
- [62] ALICE Collaboration, S. Acharya *et al.*, “ $p - p, p - \Lambda$, and $\Lambda - \Lambda$ correlations studied via femtoscopy in pp reactions at $\sqrt{s} = 7$ TeV”, *Phys. Rev. C* **99** (2019) 024001, arXiv:1805.12455 [nucl-ex].
- [63] L. Fabbietti, V. Mantovani Sarti, and O. Vazquez Doce, “Study of the Strong Interaction Among Hadrons with Correlations at the LHC”, *Ann. Rev. Nucl. Part. Sci.* **71** (2021) 377–402.
- [64] D. L. Mihaylov, V. Mantovani Sarti, O. W. Arnold, L. Fabbietti, B. Hohlweger, and A. M. Mathis, “A femtoscopic correlation analysis tool using the Schrödinger equation (CATS)”, *Eur. Phys. J. C.* **78** (2018) , arXiv:1802.08481 [nucl-ph].
- [65] R. B. Wiringa, V. G. J. Stoks, and R. Schiavilla, “An Accurate nucleon-nucleon potential with charge independence breaking”, *Phys. Rev. C* **51** (1995) 38–51, arXiv:nucl-th/9408016.
- [66] ALICE Collaboration, S. Acharya *et al.*, “Exploring the $\Lambda\bar{\Lambda}$ – $\Sigma\bar{\Sigma}$ coupled system with high precision correlation techniques at the LHC”, *Phys. Lett. B* **833** (2022) 137272, arXiv:2104.04427 [nucl-ex].
- [67] Haidenbauer, J. and Petschauer, S. and Kaiser, N. and Meissner, U. -G. and Nogga, A. and Weise, W., “Hyperon-nucleon interaction at next-to-leading order in chiral effective field theory”, *Nucl. Phys. A* **915** (2013) 24–58, arXiv:1304.5339 [nucl-th].
- [68] Haidenbauer, J. and Meißner, U. -G. and Nogga, A., “Hyperon–nucleon interaction within chiral effective field theory revisited”, *Eur. Phys. J. A* **56** (2020) 91, arXiv:1906.11681 [nucl-th].

- [69] ALICE Collaboration, S. Acharya *et al.*, “ $p - p$, $p - \Lambda$, and $\Lambda - \Lambda$ correlations studied via femtoscopy in pp reactions at $\sqrt{s} = 7$ TeV”, *Phys. Rev. C* **99** (2019) 024001, arXiv:1805.12455 [nucl-ex].
- [70] A. Kisiel, H. Zbroszczyk, and M. Szymański, “Extracting baryon-antibaryon strong-interaction potentials from $p\bar{\Lambda}$ femtoscopic correlation functions”, *Phys. Rev. C* **89** (2014) 054916, arXiv:1403.0433 [nucl-th].
- [71] B. Efron, “Bootstrap Methods: Another Look at the Jackknife”, *Ann. Statist.* **7** (1979) 1 – 26.
- [72] B. S. Pudliner, V. R. Pandharipande, J. Carlson, and R. B. Wiringa, “Quantum Monte Carlo Calculations of $A \leq 6$ Nuclei”, *Phys. Rev. Lett.* **74** (1995) 4396–4399.
- [73] ALICE Collaboration, S. Acharya *et al.*, “Anisotropic flow of identified particles in Pb–Pb collisions at $\sqrt{s_{NN}} = 5.02$ TeV”, *JHEP* **2018** (2018) , arXiv:1805.04390 [nucl-ex].
- [74] ALICE Collaboration, S. Acharya *et al.*, “Accessing the deuteron source with pion-deuteron femtoscopy in Pb-Pb collisions at $\sqrt{s_{NN}} = 5.02$ TeV”, (2025) , arXiv:2504.02333 [hep-ex].
- [75] A. Kievsky, S. Rosati, M. Viviani, L. E. Marcucci, and L. Girlanda, “A high-precision variational approach to three- and four-nucleon bound and zero-energy scattering states”, *J. Phys. G: Nucl. Part. Phys.* **35** (2008) 063101, arXiv:0805.4688 [nucl-th].
- [76] L. E. Marcucci, J. Dohet-Eraly, L. Girlanda, A. Gnech, A. Kievsky, and M. Viviani, “The Hyperspherical Harmonics method: a tool for testing and improving nuclear interaction models”, *Front. in Phys.* **8** (2020) 69, arXiv:1912.09751 [nucl-th].
- [77] Van Oers, W. T. H. and Brockman, K. W., “Phase-shift analysis of elastic nucleon-deuteron scattering”, *Nucl. Phys. A* **92** (1967) 561–583.
- [78] J. Arvieux, “Phase-shift analysis of elastic proton-deuteron scattering cross sections and ${}^3\text{He}$ excited states”, *Nucl. Phys. A* **221** (1974) 253–268.
- [79] T. Black, H. Karwowski, E. Ludwig, A. Kievsky, S. Rosati, and M. Viviani, “Determination of proton-deuteron scattering lengths”, *Phys. Lett. B* **471** (1999) 103–107.
- [80] E. Huttel, W. Arnold, H. Baumgart, H. Berg, and G. Clausnitzer, “Phase-shift analysis of pd elastic scattering below break-up threshold”, *Nucl. Phys. A* **406** (1983) 443–455.
- [81] A. Kievsky, S. Rosati, M. Viviani, C. R. Brune, H. J. Karwowski, E. J. Ludwig, and M. H. Wood, “The Three nucleon system near the N-d threshold”, *Phys. Lett. B* **406** (1997) 292–296, arXiv:nucl-th/9706077.
- [82] W. Rzeszotarski, M. Stefaniak, and S. Pratt, “Theoretical description of proton-deuteron interactions using exact two-body dynamics of the femtoscopic correlation method”, *Phys. Rev. C* **111** (2025) 034903, arXiv:2410.13983 [nucl-th].
- [83] ALICE Collaboration, W. H. Trzaska, “New ALICE detectors for Run 3 and 4 at the CERN LHC”, *Nucl. Instrum. Meth. A* **958** (2020) 162116.
- [84] Vázquez Doce, Oton and Mihaylov, Dimitar and Fabbietti, Laura, “Study of the deuterons emission time in pp collisions at the LHC via kaon-deuteron correlations”, *Eur. Phys. J. A* **61** (2025) 53, arXiv:2412.04562 [nucl-ex].
- [85] S. Mrówczyński and P. Słoń, “Deuteron-deuteron correlation function in nucleus-nucleus collisions”, *Phys. Rev. C* **104** (2021) 024909, arXiv:2103.15761 [nucl-th].

A Scaling parameters

The parameters of the fits to the femtoscopic source sizes of protons shown in Fig. 2 are summarized in Tab. A.1 and A.2. Table A.1 presents the values of the parameters a , b , and c of the power-law function fit to R_p as a function of transverse mass: $R_p = a + b \cdot \langle m_T \rangle^c$. Table A.2 presents the values of the parameters A and B of the linear function fit to the R_p as a function of $\langle dN_{ch}/d\eta \rangle^{1/3}$: $R_p = A \cdot \langle dN_{ch}/d\eta \rangle^{1/3} + B$.

Table A.1: The fitting parameters of the power-law function $R_p = a + b \cdot \langle m_T \rangle^c$, obtained from the m_T -scaling of the proton source size R_p shown in Fig. 2-(a).

Centrality	a	b	c
0–10%	3.59 ± 0.05	2.78 ± 0.04	-1.91 ± 0.09
10–30%	3.38 ± 0.02	2.21 ± 0.08	-3.16 ± 0.14
30–50%	2.50 ± 0.03	1.28 ± 0.03	-2.13 ± 0.14

Table A.2: The fitting parameters in the linear function $R_p = A \cdot \langle dN_{ch}/d\eta \rangle^{1/3} + B$, obtained for the $\langle dN_{ch}/d\eta \rangle^{1/3}$ -scaling of the proton source size R_p in Fig. 2-(b).

m_T (GeV/ c^2)	A	B
[1.0, 1.3)	0.496 ± 0.002	-0.39 ± 0.02
[1.3, 1.4)	0.428 ± 0.001	-0.05 ± 0.01
[1.4, 1.5)	0.392 ± 0.001	0.14 ± 0.01
[1.5, 1.6)	0.390 ± 0.001	0.07 ± 0.01
[1.6, 1.7)	0.388 ± 0.001	0.02 ± 0.01
[1.7, 1.8)	0.355 ± 0.001	0.25 ± 0.01
[1.8, 2.0)	0.341 ± 0.001	0.26 ± 0.01
[2.0, 3.2)	0.314 ± 0.001	0.39 ± 0.01

A The ALICE Collaboration

S. Acharya ⁵¹, G. Aglieri Rinella ³³, L. Aglietta ²⁴, M. Agnello ³⁰, N. Agrawal ²⁵, Z. Ahammed ¹³⁵, S. Ahmad ¹⁵, S.U. Ahn ⁷³, I. Ahuja ³⁷, ZUL. Akbar⁸³, A. Akindinov ¹⁴¹, V. Akishina³⁹, M. Al-Turany ⁹⁸, D. Aleksandrov ¹⁴¹, B. Alessandro ⁵⁸, H.M. Alfanda ⁶, R. Alfaro Molina ⁶⁹, B. Ali ¹⁵, A. Alici ²⁵, N. Alizadehvandchali ¹¹⁶, A. Alkin ¹⁰⁵, J. Alme ²⁰, G. Alocco ²⁴, T. Alt ⁶⁶, A.R. Altamura ⁵¹, I. Altsybeev ⁹⁶, M.N. Anaam ⁶, C. Andrei ⁴⁶, N. Andreou ¹¹⁵, A. Andronic ¹²⁶, E. Andronov ¹⁴¹, V. Anguelov ⁹⁵, F. Antinori ⁵⁵, P. Antonioli ⁵², N. Apadula ⁷⁵, H. Appelshäuser ⁶⁶, C. Arata ⁷⁴, S. Arcelli ²⁵, R. Arnaldi ⁵⁸, J.G.M.C.A. Arneiro ¹¹¹, I.C. Arsene ¹⁹, M. Arslanbekov ¹³⁸, A. Augustinus ³³, R. Averbeck ⁹⁸, D. Averyanov ¹⁴¹, M.D. Azmi ¹⁵, H. Baba¹²⁴, A. Badalà ⁵⁴, J. Bae ¹⁰⁵, Y. Bae ¹⁰⁵, Y.W. Baek ⁴¹, X. Bai ¹²⁰, R. Bailhache ⁶⁶, Y. Bailung ⁴⁹, R. Bala ⁹², A. Baldissari ¹³⁰, B. Balis ², S. Bangalia¹¹⁸, Z. Banoo ⁹², V. Barbasova ³⁷, F. Barile ³², L. Barioglio ⁵⁸, M. Barlou ⁷⁹, B. Barman ⁴², G.G. Barnaföldi ⁴⁷, L.S. Barnby ¹¹⁵, E. Barreau ¹⁰⁴, V. Barret ¹²⁷, L. Barreto ¹¹¹, K. Barth ³³, E. Bartsch ⁶⁶, N. Bastid ¹²⁷, S. Basu ^{1,76}, G. Batigne ¹⁰⁴, D. Battistini ⁹⁶, B. Batyunya ¹⁴², D. Bauri ⁴⁸, J.L. Bazo Alba ¹⁰², I.G. Bearden ⁸⁴, P. Becht ⁹⁸, D. Behera ⁴⁹, I. Belikov ¹²⁹, V.D. Bella ¹²⁹, F. Bellini ²⁵, R. Bellwied ¹¹⁶, S. Belokurova ¹⁴¹, L.G.E. Beltran ¹¹⁰, Y.A.V. Beltran ⁴⁵, G. Bencedi ⁴⁷, A. Bensaoula ¹¹⁶, S. Beole ²⁴, Y. Berdnikov ¹⁴¹, A. Berdnikova ⁹⁵, L. Bergmann ⁹⁵, L. Bernardinis ²³, L. Betev ³³, P.P. Bhaduri ¹³⁵, T. Bhalla⁹¹, A. Bhasin ⁹², B. Bhattacharjee ⁴², S. Bhattarai¹¹⁸, L. Bianchi ²⁴, J. Bielčík ³⁵, J. Bielčíková ⁸⁷, A.P. Bigot ¹²⁹, A. Bilandžić ⁹⁶, A. Binoy ¹¹⁸, G. Biro ⁴⁷, S. Biswas ⁴, D. Blau ¹⁴¹, M.B. Blidaru ⁹⁸, N. Bluhme³⁹, C. Blume ⁶⁶, F. Bock ⁸⁸, T. Bodova ²⁰, J. Bok ¹⁶, L. Boldizsár ⁴⁷, M. Bombara ³⁷, P.M. Bond ³³, G. Bonomi ^{134,56}, H. Borel ¹³⁰, A. Borissov ¹⁴¹, A.G. Borquez Carcamo ⁹⁵, E. Botta ²⁴, Y.E.M. Bouziani ⁶⁶, D.C. Brandibur ⁶⁵, L. Bratrud ⁶⁶, P. Braun-Munzinger ⁹⁸, M. Bregant ¹¹¹, M. Broz ³⁵, G.E. Bruno ^{97,32}, V.D. Buchakchiev ³⁶, M.D. Buckland ⁸⁶, D. Budnikov ¹⁴¹, H. Buesching ⁶⁶, S. Bufalino ³⁰, P. Buhler ¹⁰³, N. Burmasov ¹⁴¹, Z. Buthelezi ^{70,123}, A. Bylinkin ²⁰, S.A. Bysiak ¹⁰⁸, C. Carr ¹⁰¹, J.C. Cabanillas Noris ¹¹⁰, M.F.T. Cabrera ¹¹⁶, H. Caines ¹³⁸, A. Caliva ²⁹, E. Calvo Villar ¹⁰², J.M.M. Camacho ¹¹⁰, P. Camerini ²³, M.T. Camerlingo ⁵¹, F.D.M. Canedo ¹¹¹, S. Cannito ²³, S.L. Cantway ¹³⁸, M. Carabas ¹¹⁴, F. Carnesecchi ³³, L.A.D. Carvalho ¹¹¹, J. Castillo Castellanos ¹³⁰, M. Castoldi ³³, F. Catalano ³³, S. Cattaruzzi ²³, R. Cerri ²⁴, I. Chakaberia ⁷⁵, P. Chakraborty ¹³⁶, S. Chandra ¹³⁵, S. Chapelard ³³, M. Chartier ¹¹⁹, S. Chattopadhyay¹³⁵, M. Chen ⁴⁰, T. Cheng ⁶, C. Cheshkov ¹²⁸, D. Chiappara ²⁷, V. Chibante Barroso ³³, D.D. Chinellato ¹⁰³, F. Chinu ²⁴, E.S. Chizzali ^{II,96}, J. Cho ⁶⁰, S. Cho ⁶⁰, P. Chochula ³³, Z.A. Chochulska¹³⁶, D. Choudhury⁴², S. Choudhury¹⁰⁰, P. Christakoglou ⁸⁵, C.H. Christensen ⁸⁴, P. Christiansen ⁷⁶, T. Chujo ¹²⁵, M. Ciacco ³⁰, C. Ciccalo ⁵³, G. Cimador ²⁴, F. Cindolo ⁵², M.R. Ciupek⁹⁸, G. Clai^{III,52}, F. Colamaria ⁵¹, J.S. Colburn¹⁰¹, D. Colella ³², A. Colelli³², M. Colocci ²⁵, M. Concias ³³, G. Conesa Balbastre ⁷⁴, Z. Conesa del Valle ¹³¹, G. Contin ²³, J.G. Contreras ³⁵, M.L. Coquet ¹⁰⁴, P. Cortese ^{133,58}, M.R. Cosentino ¹¹³, F. Costa ³³, S. Costanza ²¹, P. Crochet ¹²⁷, M.M. Czarnynoga¹³⁶, A. Dainese ⁵⁵, G. Dange³⁹, M.C. Danisch ⁹⁵, A. Danu ⁶⁵, P. Das ³³, S. Das ⁴, A.R. Dash ¹²⁶, S. Dash ⁴⁸, A. De Caro ²⁹, G. de Cataldo ⁵¹, J. de Cuveland ³⁹, A. De Falco ²², D. De Gruttola ²⁹, N. De Marco ⁵⁸, C. De Martin ²³, S. De Pasquale ²⁹, R. Deb ¹³⁴, R. Del Grande ⁹⁶, L. Dello Stritto ³³, G.G.A. de Souza ^{IV,111}, P. Dhankher ¹⁸, D. Di Bari ³², M. Di Costanzo ³⁰, A. Di Mauro ³³, B. Di Ruzza ¹³², B. Diab ³³, R.A. Diaz ¹⁴², Y. Ding ⁶, J. Ditzel ⁶⁶, R. Divià ³³, Ø. Djupsland²⁰, U. Dmitrieva ¹⁴¹, A. Dobrin ⁶⁵, B. Döningus ⁶⁶, L. Döpper ⁴³, J.M. Dubinski ¹³⁶, A. Dubla ⁹⁸, P. Dupieux ¹²⁷, N. Dzalaiova¹³, T.M. Eder ¹²⁶, R.J. Ehlers ⁷⁵, F. Eisenhut ⁶⁶, R. Ejima ⁹³, D. Elia ⁵¹, B. Erazmus ¹⁰⁴, F. Ercolelli ²⁵, B. Espagnon ¹³¹, G. Eulisse ³³, D. Evans ¹⁰¹, S. Evdokimov ¹⁴¹, L. Fabbietti ⁹⁶, M. Faggin ³³, J. Faivre ⁷⁴, F. Fan ⁶, W. Fan ⁷⁵, T. Fang⁶, A. Fantoni ⁵⁰, M. Fasel ⁸⁸, G. Feofilov ¹⁴¹, A. Fernández Téllez ⁴⁵, L. Ferrandi ¹¹¹, M.B. Ferrer ³³, A. Ferrero ¹³⁰, C. Ferrero ^{V,58}, A. Ferretti ²⁴, V.J.G. Feuillard ⁹⁵, D. Finogeev ¹⁴¹, F.M. Fionda ⁵³, F. Flor ¹³⁸, A.N. Flores ¹⁰⁹, S. Foertsch ⁷⁰, I. Fokin ⁹⁵, S. Fokin ¹⁴¹, U. Follo ^{V,58}, R. Forynski ¹¹⁵, E. Fragiocomo ⁵⁹, E. Frajna ⁴⁷, H. Friberg ⁹⁶, U. Fuchs ³³, N. Funicello ²⁹, C. Furget ⁷⁴, A. Furs ¹⁴¹, T. Fusayasu ⁹⁹, J.J. Gaardhøje ⁸⁴, M. Gagliardi ²⁴, A.M. Gago ¹⁰², T. Gahlaut⁴⁸, C.D. Galvan ¹¹⁰, S. Gami⁸¹, D.R. Gangadharian ¹¹⁶, P. Ganoti ⁷⁹, C. Garabatos ⁹⁸, J.M. Garcia ⁴⁵, T. García Chávez ⁴⁵, E. Garcia-Solis ⁹, S. Garetti¹³¹, C. Gargiulo ³³, P. Gasik ⁹⁸, H.M. Gaur³⁹, A. Gautam ¹¹⁸, M.B. Gay Ducati ⁶⁸, M. Germain ¹⁰⁴, R.A. Gernhaeuser ⁹⁶, C. Ghosh¹³⁵, M. Giacalone ⁵², G. Gioachin ³⁰, S.K. Giri ¹³⁵, P. Giubellino ^{98,58}, P. Giubilato ²⁷, A.M.C. Glaenzer ¹³⁰, P. Glässel ⁹⁵, E. Glimos ¹²², V. Gonzalez ¹³⁷, P. Gordeev ¹⁴¹, M. Gorgon ², K. Goswami ⁴⁹, S. Gotovac ³⁴, V. Grabski ⁶⁹, L.K. Graczykowski ¹³⁶, E. Grecka ⁸⁷, A. Grelli ⁶¹, C. Grigoras ³³, V. Grigoriev ¹⁴¹, S. Grigoryan ^{142,1},

O.S. Groettvik $\textcircled{33}$, F. Grossa $\textcircled{33}$, J.F. Grosse-Oetringhaus $\textcircled{33}$, R. Grossos $\textcircled{98}$, D. Grund $\textcircled{35}$, N.A. Grunwald $\textcircled{95}$, R. Guernane $\textcircled{74}$, M. Guilbaud $\textcircled{104}$, K. Gulbrandsen $\textcircled{84}$, J.K. Gumprecht $\textcircled{103}$, T. Gündem $\textcircled{66}$, T. Gunji $\textcircled{124}$, J. Guo $\textcircled{10}$, W. Guo $\textcircled{6}$, A. Gupta $\textcircled{92}$, R. Gupta $\textcircled{92}$, R. Gupta $\textcircled{49}$, K. Gwizdziel $\textcircled{136}$, L. Gyulai $\textcircled{47}$, C. Hadjidakis $\textcircled{131}$, F.U. Haider $\textcircled{92}$, S. Haidlova $\textcircled{35}$, M. Haldar $\textcircled{4}$, H. Hamagaki $\textcircled{77}$, Y. Han $\textcircled{140}$, B.G. Hanley $\textcircled{137}$, R. Hannigan $\textcircled{109}$, J. Hansen $\textcircled{76}$, J.W. Harris $\textcircled{138}$, A. Harton $\textcircled{9}$, M.V. Hartung $\textcircled{66}$, H. Hassan $\textcircled{117}$, D. Hatzifotiadou $\textcircled{52}$, P. Hauer $\textcircled{43}$, L.B. Havener $\textcircled{138}$, E. Hellbär $\textcircled{33}$, H. Helstrup $\textcircled{38}$, M. Hemmer $\textcircled{66}$, T. Herman $\textcircled{35}$, S.G. Hernandez $\textcircled{116}$, G. Herrera Corral $\textcircled{8}$, S. Herrmann $\textcircled{128}$, K.F. Hetland $\textcircled{38}$, B. Heybeck $\textcircled{66}$, H. Hillemanns $\textcircled{33}$, B. Hippolyte $\textcircled{129}$, I.P.M. Hobus $\textcircled{85}$, F.W. Hoffmann $\textcircled{72}$, B. Hofman $\textcircled{61}$, M. Horst $\textcircled{96}$, A. Horzyk $\textcircled{2}$, Y. Hou $\textcircled{6}$, P. Hristov $\textcircled{33}$, P. Huhn $\textcircled{66}$, L.M. Huhta $\textcircled{117}$, T.J. Humanic $\textcircled{89}$, V. Humlova $\textcircled{35}$, A. Hutson $\textcircled{116}$, D. Hutter $\textcircled{39}$, M.C. Hwang $\textcircled{18}$, R. Ilkaev $\textcircled{141}$, M. Inaba $\textcircled{125}$, M. Ippolitov $\textcircled{141}$, A. Isakov $\textcircled{85}$, T. Isidori $\textcircled{118}$, M.S. Islam $\textcircled{48}$, S. Iurchenko $\textcircled{141}$, M. Ivanov $\textcircled{98}$, M. Ivanov $\textcircled{13}$, V. Ivanov $\textcircled{141}$, K.E. Iversen $\textcircled{76}$, J.G. Kim $\textcircled{140}$, M. Jablonski $\textcircled{2}$, B. Jacak $\textcircled{18,75}$, N. Jacazio $\textcircled{25}$, P.M. Jacobs $\textcircled{75}$, S. Jadlovska $\textcircled{107}$, J. Jadlovsky $\textcircled{107}$, S. Jaelani $\textcircled{83}$, C. Jahnke $\textcircled{112}$, M.J. Jakubowska $\textcircled{136}$, M.A. Janik $\textcircled{136}$, S. Ji $\textcircled{16}$, S. Jia $\textcircled{10}$, T. Jiang $\textcircled{10}$, A.A.P. Jimenez $\textcircled{67}$, S. Jin $\textcircled{1,10}$, F. Jonas $\textcircled{75}$, D.M. Jones $\textcircled{119}$, J.M. Jowett $\textcircled{33,98}$, J. Jung $\textcircled{66}$, M. Jung $\textcircled{66}$, A. Junique $\textcircled{33}$, A. Jusko $\textcircled{101}$, J. Kaewjai $\textcircled{106}$, P. Kalinak $\textcircled{62}$, A. Kalweit $\textcircled{33}$, A. Karasu Uysal $\textcircled{139}$, N. Karatzenis $\textcircled{101}$, O. Karavichev $\textcircled{141}$, T. Karavicheva $\textcircled{141}$, E. Karpechev $\textcircled{141}$, M.J. Karwowska $\textcircled{136}$, U. Kebschull $\textcircled{72}$, M. Keil $\textcircled{33}$, B. Ketzer $\textcircled{43}$, J. Keul $\textcircled{66}$, S.S. Khade $\textcircled{49}$, A.M. Khan $\textcircled{120}$, S. Khan $\textcircled{15}$, A. Khanzadeev $\textcircled{141}$, Y. Kharlov $\textcircled{141}$, A. Khatun $\textcircled{118}$, A. Khuntia $\textcircled{52}$, Z. Khuranova $\textcircled{66}$, A. Kievsky $\textcircled{57}$, B. Kileng $\textcircled{38}$, B. Kim $\textcircled{105}$, C. Kim $\textcircled{16}$, D.J. Kim $\textcircled{117}$, D. Kim $\textcircled{105}$, E.J. Kim $\textcircled{71}$, G. Kim $\textcircled{60}$, H. Kim $\textcircled{60}$, J. Kim $\textcircled{140}$, J. Kim $\textcircled{60}$, J. Kim $\textcircled{33}$, M. Kim $\textcircled{18}$, S. Kim $\textcircled{17}$, T. Kim $\textcircled{140}$, K. Kimura $\textcircled{93}$, S. Kirsch $\textcircled{66}$, I. Kisel $\textcircled{39}$, S. Kiselev $\textcircled{141}$, A. Kisiel $\textcircled{136}$, J.L. Klay $\textcircled{5}$, J. Klein $\textcircled{33}$, S. Klein $\textcircled{75}$, C. Klein-Bösing $\textcircled{126}$, M. Kleiner $\textcircled{66}$, T. Klemenz $\textcircled{96}$, A. Kluge $\textcircled{33}$, C. Kobdaj $\textcircled{106}$, R. Kohara $\textcircled{124}$, T. Kollegger $\textcircled{98}$, A. Kondratyev $\textcircled{142}$, N. Kondratyeva $\textcircled{141}$, J. Konig $\textcircled{66}$, P.J. Konopka $\textcircled{33}$, G. Kornakov $\textcircled{136}$, M. Korwieser $\textcircled{96}$, S.D. Koryciak $\textcircled{2}$, C. Koster $\textcircled{85}$, A. Kotliarov $\textcircled{87}$, N. Kovacic $\textcircled{90}$, V. Kovalenko $\textcircled{141}$, M. Kowalski $\textcircled{108}$, V. Kozhuharov $\textcircled{36}$, G. Kozlov $\textcircled{39}$, I. Králik $\textcircled{62}$, A. Kravčáková $\textcircled{37}$, L. Krcal $\textcircled{33}$, M. Krivda $\textcircled{101,62}$, F. Krizek $\textcircled{87}$, K. Krizkova Gajdosova $\textcircled{35}$, C. Krug $\textcircled{68}$, M. Krüger $\textcircled{66}$, D.M. Krupova $\textcircled{35}$, E. Kryshen $\textcircled{141}$, V. Kučera $\textcircled{60}$, C. Kuhn $\textcircled{129}$, P.G. Kuijer $\textcircled{85}$, T. Kumaoka $\textcircled{125}$, D. Kumar $\textcircled{135}$, L. Kumar $\textcircled{91}$, N. Kumar $\textcircled{91}$, S. Kumar $\textcircled{51}$, S. Kundu $\textcircled{33}$, M. Kuo $\textcircled{125}$, P. Kurashvili $\textcircled{80}$, A.B. Kurepin $\textcircled{141}$, S. Kurita $\textcircled{93}$, A. Kuryakin $\textcircled{141}$, S. Kushpil $\textcircled{87}$, V. Kuskov $\textcircled{141}$, M. Kutyla $\textcircled{136}$, A. Kuznetsov $\textcircled{142}$, M.J. Kweon $\textcircled{60}$, Y. Kwon $\textcircled{140}$, S.L. La Pointe $\textcircled{39}$, P. La Rocca $\textcircled{26}$, A. Lakrathok $\textcircled{106}$, M. Lamanna $\textcircled{33}$, S. Lambert $\textcircled{104}$, A.R. Landou $\textcircled{74}$, R. Langoy $\textcircled{121}$, P. Larionov $\textcircled{33}$, E. Laudi $\textcircled{33}$, L. Lautner $\textcircled{96}$, R.A.N. Laveaga $\textcircled{110}$, R. Lavicka $\textcircled{103}$, R. Lea $\textcircled{134,56}$, H. Lee $\textcircled{105}$, I. Legrand $\textcircled{46}$, G. Legras $\textcircled{126}$, A.M. Lejeune $\textcircled{35}$, T.M. Lelek $\textcircled{2}$, R.C. Lemmon $\textcircled{1,86}$, I. León Monzón $\textcircled{110}$, M.M. Lesch $\textcircled{96}$, P. Lévai $\textcircled{47}$, M. Li $\textcircled{6}$, P. Li $\textcircled{10}$, X. Li $\textcircled{10}$, B.E. Liang-Gilman $\textcircled{18}$, J. Lien $\textcircled{121}$, R. Lietava $\textcircled{101}$, I. Likmeta $\textcircled{116}$, B. Lim $\textcircled{24}$, H. Lim $\textcircled{16}$, S.H. Lim $\textcircled{16}$, S. Lin $\textcircled{10}$, V. Lindenstruth $\textcircled{39}$, C. Lippmann $\textcircled{98}$, D. Liskova $\textcircled{107}$, D.H. Liu $\textcircled{6}$, J. Liu $\textcircled{119}$, G.S.S. Liveraro $\textcircled{112}$, I.M. Lofnes $\textcircled{20}$, C. Loizides $\textcircled{88}$, S. Lokos $\textcircled{108}$, J. Lömker $\textcircled{61}$, X. Lopez $\textcircled{127}$, E. López Torres $\textcircled{7}$, C. Lotteau $\textcircled{128}$, P. Lu $\textcircled{98,120}$, W. Lu $\textcircled{6}$, Z. Lu $\textcircled{10}$, F.V. Lugo $\textcircled{69}$, J. Luo $\textcircled{40}$, G. Luparello $\textcircled{59}$, M.A.T. Johnson $\textcircled{45}$, Y.G. Ma $\textcircled{40}$, M. Mager $\textcircled{33}$, A. Maire $\textcircled{129}$, E.M. Majerz $\textcircled{2}$, M.V. Makarieva $\textcircled{36}$, M. Malaev $\textcircled{141}$, G. Malfattore $\textcircled{52,25}$, N.M. Malik $\textcircled{92}$, N. Malik $\textcircled{15}$, S.K. Malik $\textcircled{92}$, D. Mallick $\textcircled{131}$, N. Mallick $\textcircled{117}$, G. Mandaglio $\textcircled{31,54}$, S.K. Mandal $\textcircled{80}$, A. Manea $\textcircled{65}$, V. Manko $\textcircled{141}$, A.K. Manna $\textcircled{49}$, F. Manso $\textcircled{127}$, G. Mantzaridis $\textcircled{96}$, V. Manzari $\textcircled{51}$, Y. Mao $\textcircled{6}$, R.W. Marcjan $\textcircled{2}$, L.E. Marcucci $\textcircled{27}$, G.V. Margagliotti $\textcircled{23}$, A. Margotti $\textcircled{52}$, A. Marín $\textcircled{98}$, C. Markert $\textcircled{109}$, P. Martinengo $\textcircled{33}$, M.I. Martínez $\textcircled{45}$, G. Martínez García $\textcircled{104}$, M.P.P. Martins $\textcircled{33,111}$, S. Masciocchi $\textcircled{98}$, M. Masera $\textcircled{24}$, A. Masoni $\textcircled{53}$, L. Massacrier $\textcircled{131}$, O. Massen $\textcircled{61}$, A. Mastroserio $\textcircled{132,51}$, L. Mattei $\textcircled{24,127}$, S. Mattiazzzo $\textcircled{27}$, A. Matyja $\textcircled{108}$, F. Mazzaschi $\textcircled{33}$, M. Mazzilli $\textcircled{116}$, Y. Melikyan $\textcircled{44}$, M. Melo $\textcircled{111}$, A. Menchaca-Rocha $\textcircled{69}$, J.E.M. Mendez $\textcircled{67}$, E. Meninno $\textcircled{103}$, A.S. Menon $\textcircled{116}$, M.W. Menzel $\textcircled{33,95}$, M. Meres $\textcircled{13}$, L. Micheletti $\textcircled{58}$, D. Mihai $\textcircled{114}$, D.L. Mihaylov $\textcircled{96}$, A.U. Mikalsen $\textcircled{20}$, K. Mikhaylov $\textcircled{142,141}$, N. Minafra $\textcircled{118}$, D. Miśkowiec $\textcircled{98}$, A. Modak $\textcircled{59,134}$, B. Mohanty $\textcircled{81}$, M. Mohisin Khan $\textcircled{VI,15}$, M.A. Molander $\textcircled{44}$, M.M. Mondal $\textcircled{81}$, S. Monira $\textcircled{136}$, D.A. Moreira De Godoy $\textcircled{126}$, I. Morozov $\textcircled{141}$, A. Morsch $\textcircled{33}$, T. Mrnjavac $\textcircled{33}$, S. Mrozninski $\textcircled{66}$, V. Muccifora $\textcircled{50}$, S. Muhuri $\textcircled{135}$, A. Mulliri $\textcircled{22}$, M.G. Munhoz $\textcircled{111}$, R.H. Munzer $\textcircled{66}$, H. Murakami $\textcircled{124}$, L. Musa $\textcircled{33}$, J. Musinsky $\textcircled{62}$, J.W. Myrcha $\textcircled{136}$, N.B. Sundstrom $\textcircled{61}$, B. Naik $\textcircled{123}$, A.I. Nambrath $\textcircled{18}$, B.K. Nandi $\textcircled{48}$, R. Nania $\textcircled{52}$, E. Nappi $\textcircled{51}$, A.F. Nassirpour $\textcircled{17}$, V. Nastase $\textcircled{114}$, A. Nath $\textcircled{95}$, N.F. Nathanson $\textcircled{84}$, C. Natrass $\textcircled{122}$, K. Naumov $\textcircled{18}$, A. Neagu $\textcircled{19}$, L. Nellen $\textcircled{67}$, R. Nepeivoda $\textcircled{76}$, S. Nese $\textcircled{19}$, N. Nicassio $\textcircled{32}$, B.S. Nielsen $\textcircled{84}$, E.G. Nielsen $\textcircled{84}$, S. Nikolaev $\textcircled{141}$, V. Nikulin $\textcircled{141}$, F. Noferini $\textcircled{52}$, S. Noh $\textcircled{12}$, P. Nomokonov $\textcircled{142}$, J. Norman $\textcircled{119}$, N. Novitzky $\textcircled{88}$,

J. Nystrand ²⁰, M.R. Ockleton¹¹⁹, M. Ogino ⁷⁷, S. Oh ¹⁷, A. Ohlson ⁷⁶, M. Oida ⁹³, V.A. Okorokov ¹⁴¹, J. Oleniacz ¹³⁶, C. Oppedisano ⁵⁸, A. Ortiz Velasquez ⁶⁷, J. Otwinowski ¹⁰⁸, M. Oya⁹³, K. Oyama ⁷⁷, S. Padhan ⁴⁸, D. Pagano ^{134,56}, G. Paić ⁶⁷, S. Paisano-Guzmán ⁴⁵, A. Palasciano ⁵¹, I. Panasenko⁷⁶, S. Panebianco ¹³⁰, P. Panigrahi ⁴⁸, C. Pantouvakis ²⁷, H. Park ¹²⁵, J. Park ¹²⁵, S. Park ¹⁰⁵, J.E. Parkkila ³³, Y. Patley ⁴⁸, R.N. Patra⁵¹, P. Paudel¹¹⁸, B. Paul ¹³⁵, H. Pei ⁶, T. Peitzmann ⁶¹, X. Peng ¹¹, M. Pennisi ²⁴, S. Perciballi ²⁴, D. Peresunko ¹⁴¹, G.M. Perez ⁷, Y. Pestov¹⁴¹, V. Petrov ¹⁴¹, M. Petrovici ⁴⁶, S. Piano ⁵⁹, M. Pikna ¹³, P. Pillot ¹⁰⁴, O. Pinazza ^{52,33}, L. Pinsky¹¹⁶, C. Pinto ³³, S. Pisano ⁵⁰, M. Płoskoń ⁷⁵, M. Planinic ⁹⁰, D.K. Plociennik ², M.G. Poghosyan ⁸⁸, B. Polichtchouk ¹⁴¹, S. Politano ^{33,24}, N. Poljak ⁹⁰, A. Pop ⁴⁶, S. Porteboeuf-Houssais ¹²⁷, I.Y. Pozos ⁴⁵, K.K. Pradhan ⁴⁹, S.K. Prasad ⁴, S. Prasad ⁴⁹, R. Preghenella ⁵², F. Prino ⁵⁸, C.A. Pruneau ¹³⁷, I. Pshenichnov ¹⁴¹, M. Puccio ³³, S. Pucillo ^{29,24}, L. Quaglia ²⁴, A.M.K. Radhakrishnan⁴⁹, S. Ragoni ¹⁴, A. Rai ¹³⁸, A. Rakotozafindrabe ¹³⁰, N. Ramasubramanian¹²⁸, L. Ramello ^{133,58}, C.O. Ramírez-Álvarez ⁴⁵, M. Rasa ²⁶, S.S. Räsänen ⁴⁴, R. Rath ⁵², M.P. Rauch ²⁰, I. Ravasenga ³³, K.F. Read ^{88,122}, C. Reckziegel ¹¹³, A.R. Redelbach ³⁹, K. Redlich ^{VII,80}, C.A. Reetz ⁹⁸, H.D. Regules-Medel ⁴⁵, A. Rehman ²⁰, F. Reidt ³³, H.A. Reme-Ness ³⁸, K. Reygers ⁹⁵, A. Riabov ¹⁴¹, V. Riabov ¹⁴¹, R. Ricci ²⁹, M. Richter ²⁰, A.A. Riedel ⁹⁶, W. Riegler ³³, A.G. Riffero ²⁴, M. Rignanese ²⁷, C. Ripoli ²⁹, C. Ristea ⁶⁵, M.V. Rodriguez ³³, M. Rodríguez Cahuantzi ⁴⁵, K. Røed ¹⁹, R. Rogalev ¹⁴¹, E. Rogochaya ¹⁴², D. Rohr ³³, D. Röhrich ²⁰, S. Rojas Torres ³⁵, P.S. Rokita ¹³⁶, G. Romanenko ²⁵, F. Ronchetti ³³, D. Rosales Herrera ⁴⁵, E.D. Rosas⁶⁷, K. Roslon ¹³⁶, A. Rossi ⁵⁵, A. Roy ⁴⁹, S. Roy ⁴⁸, N. Rubini ⁵², J.A. Rudolph⁸⁵, D. Ruggiano ¹³⁶, R. Rui ²³, P.G. Russek ², R. Russo ⁸⁵, A. Rustamov ⁸², E. Ryabinkin ¹⁴¹, Y. Ryabov ¹⁴¹, A. Rybicki ¹⁰⁸, L.C.V. Ryder ¹¹⁸, J. Ryu ¹⁶, W. Rzesz ¹³⁶, B. Sabiu ⁵², S. Sadhu ⁴³, S. Sadovsky ¹⁴¹, J. Saetre ²⁰, S. Saha ⁸¹, B. Sahoo ⁴⁹, R. Sahoo ⁴⁹, D. Sahu ⁴⁹, P.K. Sahu ⁶³, J. Saini ¹³⁵, K. Sajdakova³⁷, S. Sakai ¹²⁵, S. Sambyal ⁹², D. Samitz ¹⁰³, I. Sanna ^{33,96}, T.B. Saramela¹¹¹, D. Sarkar ⁸⁴, P. Sarma ⁴², V. Sarritzu ²², V.M. Sarti ⁹⁶, M.H.P. Sas ³³, S. Sawan ⁸¹, E. Scapparone ⁵², J. Schambach ⁸⁸, H.S. Scheid ³³, C. Schiaua ⁴⁶, R. Schicker ⁹⁵, F. Schlepper ^{33,95}, A. Schmah⁹⁸, C. Schmidt ⁹⁸, M.O. Schmidt ³³, M. Schmidt⁹⁴, N.V. Schmidt ⁸⁸, A.R. Schmier ¹²², J. Schoengarth ⁶⁶, R. Schotter ¹⁰³, A. Schröter ³⁹, J. Schukraft ³³, K. Schweda ⁹⁸, G. Scioli ²⁵, E. Scomparin ⁵⁸, J.E. Seger ¹⁴, Y. Sekiguchi¹²⁴, D. Sekihata ¹²⁴, M. Selina ⁸⁵, I. Selyuzhenkov ⁹⁸, S. Senyukov ¹²⁹, J.J. Seo ⁹⁵, D. Serebryakov ¹⁴¹, L. Serkin ^{VIII,67}, L. Šerkšnytė ⁹⁶, A. Sevcenco ⁶⁵, T.J. Shaba ⁷⁰, A. Shabetai ¹⁰⁴, R. Shahoyan ³³, A. Shangaraev ¹⁴¹, B. Sharma ⁹², D. Sharma ⁴⁸, H. Sharma ⁵⁵, M. Sharma ⁹², S. Sharma ⁹², T. Sharma ⁴², U. Sharma ⁹², A. Shatat ¹³¹, O. Sheibani¹³⁷, K. Shigaki ⁹³, M. Shimomura ⁷⁸, S. Shirinkin ¹⁴¹, Q. Shou ⁴⁰, Y. Sibirskiak ¹⁴¹, S. Siddhanta ⁵³, T. Siemiarczuk ⁸⁰, T.F. Silva ¹¹¹, D. Silvermyr ⁷⁶, T. Simantathammakul ¹⁰⁶, R. Simeonov ³⁶, B. Singh⁹², B. Singh ⁹⁶, K. Singh ⁴⁹, R. Singh ⁸¹, R. Singh ^{55,98}, S. Singh ¹⁵, V.K. Singh ¹³⁵, V. Singhal ¹³⁵, T. Sinha ¹⁰⁰, B. Sitar ¹³, M. Sitta ^{133,58}, T.B. Skaali ¹⁹, G. Skorodumovs ⁹⁵, N. Smirnov ¹³⁸, R.J.M. Snellings ⁶¹, E.H. Solheim ¹⁹, C. Sonnabend ^{33,98}, J.M. Sonneveld ⁸⁵, F. Soramel ²⁷, A.B. Soto-hernandez ⁸⁹, R. Spijkers ⁸⁵, I. Sputowska ¹⁰⁸, J. Staa ⁷⁶, J. Stachel ⁹⁵, I. Stan ⁶⁵, T. Stellhorn ¹²⁶, S.F. Stieffelmaier ⁹⁵, D. Stocco ¹⁰⁴, I. Storehaug ¹⁹, N.J. Strangmann ⁶⁶, P. Stratmann ¹²⁶, S. Strazzi ²⁵, A. Sturniolo ^{31,54}, C.P. Stylianidis⁸⁵, A.A.P. Suaide ¹¹¹, C. Suire ¹³¹, A. Suiu ^{33,114}, M. Sukhanov ¹⁴¹, M. Suljic ³³, R. Sultanov ¹⁴¹, V. Sumberia ⁹², S. Sumowidagdo ⁸³, L.H. Tabares ⁷, S.F. Taghavi ⁹⁶, J. Takahashi ¹¹², G.J. Tambave ⁸¹, Z. Tang ¹²⁰, J. Tanwar ⁹¹, J.D. Tapia Takaki ¹¹⁸, N. Tapus ¹¹⁴, L.A. Tarasovicova ³⁷, M.G. Tarzila ⁴⁶, A. Tauro ³³, A. Tavira García ¹³¹, G. Tejeda Muñoz ⁴⁵, L. Terlizzi ²⁴, C. Terrevoli ⁵¹, D. Thakur ²⁴, S. Thakur ⁴, M. Thogersen ¹⁹, D. Thomas ¹⁰⁹, A. Tikhonov ¹⁴¹, N. Tiltmann ^{33,126}, A.R. Timmins ¹¹⁶, M. Tkacik¹⁰⁷, A. Toia ⁶⁶, R. Tokumoto⁹³, S. Tomassini ²⁵, K. Tomohiro⁹³, N. Topilskaya ¹⁴¹, M. Toppi ⁵⁰, V.V. Torres ¹⁰⁴, A. Trifiró ^{31,54}, T. Trilloki ⁹⁷, A.S. Triolo ^{33,31,54}, S. Tripathy ³³, T. Tripathy ¹²⁷, S. Trogolo ²⁴, V. Trubnikov ³, W.H. Trzaska ¹¹⁷, T.P. Trzcinski ¹³⁶, C. Tsolanta¹⁹, R. Tu⁴⁰, A. Tumkin ¹⁴¹, R. Turrisi ⁵⁵, T.S. Tveter ¹⁹, K. Ullaland ²⁰, B. Ulukutlu ⁹⁶, S. Upadhyaya ¹⁰⁸, A. Uras ¹²⁸, M. Urioni ²³, G.L. Usai ²², M. Vaid⁹², M. Vala ³⁷, N. Valle ⁵⁶, L.V.R. van Doremalen⁶¹, M. van Leeuwen ⁸⁵, C.A. van Veen ⁹⁵, R.J.G. van Weelden ⁸⁵, D. Varga ⁴⁷, Z. Varga ¹³⁸, P. Vargas Torres⁶⁷, M. Vasileiou ⁷⁹, A. Vasiliev ^{I,141}, O. Vázquez Doce ⁵⁰, O. Vazquez Rueda ¹¹⁶, V. Vechernin ¹⁴¹, P. Veen ¹³⁰, E. Vercellin ²⁴, R. Verma ⁴⁸, R. Vértesi ⁴⁷, M. Verweij ⁶¹, L. Vickovic³⁴, Z. Vilakazi¹²³, O. Villalobos Baillie ¹⁰¹, A. Villani ²³, A. Vinogradov ¹⁴¹, T. Virgili ²⁹, M.M.O. Virta ¹¹⁷, M. Viviani ⁵⁷, A. Vodopyanov ¹⁴², B. Volkel ³³, M.A. Völk ¹⁰¹, S.A. Voloshin ¹³⁷, G. Volpe ³², B. von Haller ³³, I. Vorobyev ³³, N. Vozniuk ¹⁴¹, J. Vrláková ³⁷, J. Wan⁴⁰, C. Wang ⁴⁰,

D. Wang ⁴⁰, Y. Wang ⁴⁰, Y. Wang ⁶, Z. Wang ⁴⁰, A. Wegrzynek ³³, F. Weiglhofer ³⁹, S.C. Wenzel ³³, J.P. Wessels ¹²⁶, P.K. Wiacek ², J. Wiechula ⁶⁶, J. Wikne ¹⁹, G. Wilk ⁸⁰, J. Wilkinson ⁹⁸, G.A. Willems ¹²⁶, B. Windelband ⁹⁵, M. Winn ¹³⁰, J. Witte ⁹⁸, J.R. Wright ¹⁰⁹, C. Wu⁵⁵, W. Wu⁴⁰, Y. Wu ¹²⁰, K. Xiong⁴⁰, Z. Xiong¹²⁰, L. Xu⁶, R. Xu ⁶, A. Yadav ⁴³, A.K. Yadav ¹³⁵, Y. Yamaguchi ⁹³, S. Yang ⁶⁰, S. Yang ²⁰, S. Yano ⁹³, E.R. Yeats¹⁸, J. Yi ⁶, Z. Yin ⁶, I.-K. Yoo ¹⁶, J.H. Yoon ⁶⁰, H. Yu ¹², S. Yuan²⁰, A. Yuncu ⁹⁵, V. Zaccolo ²³, C. Zampolli ³³, F. Zanone ⁹⁵, N. Zardoshti ³³, P. Závada ⁶⁴, M. Zhalov ¹⁴¹, B. Zhang ⁹⁵, C. Zhang ¹³⁰, L. Zhang ⁴⁰, M. Zhang ^{127,6}, M. Zhang ^{27,6}, S. Zhang ⁴⁰, X. Zhang ⁶, Y. Zhang¹²⁰, Y. Zhang ¹²⁰, Z. Zhang ⁶, M. Zhao ¹⁰, V. Zhrebchevskii ¹⁴¹, Y. Zhi¹⁰, D. Zhou ⁶, Y. Zhou ⁸⁴, J. Zhu ^{55,6}, S. Zhu^{98,120}, Y. Zhu⁶, S.C. Zugravel ⁵⁸, N. Zurlo ^{134,56}

Affiliation Notes

^I Deceased

^{II} Also at: Max-Planck-Institut fur Physik, Munich, Germany

^{III} Also at: Italian National Agency for New Technologies, Energy and Sustainable Economic Development (ENEA), Bologna, Italy

^{IV} Also at: Instituto de Fisica da Universidade de Sao Paulo

^V Also at: Dipartimento DET del Politecnico di Torino, Turin, Italy

^{VI} Also at: Department of Applied Physics, Aligarh Muslim University, Aligarh, India

^{VII} Also at: Institute of Theoretical Physics, University of Wroclaw, Poland

^{VIII} Also at: Facultad de Ciencias, Universidad Nacional Autónoma de México, Mexico City, Mexico

Collaboration Institutes

¹ A.I. Alikhanyan National Science Laboratory (Yerevan Physics Institute) Foundation, Yerevan, Armenia

² AGH University of Krakow, Cracow, Poland

³ Bogolyubov Institute for Theoretical Physics, National Academy of Sciences of Ukraine, Kiev, Ukraine

⁴ Bose Institute, Department of Physics and Centre for Astroparticle Physics and Space Science (CAPSS), Kolkata, India

⁵ California Polytechnic State University, San Luis Obispo, California, United States

⁶ Central China Normal University, Wuhan, China

⁷ Centro de Aplicaciones Tecnológicas y Desarrollo Nuclear (CEADEN), Havana, Cuba

⁸ Centro de Investigación y de Estudios Avanzados (CINVESTAV), Mexico City and Mérida, Mexico

⁹ Chicago State University, Chicago, Illinois, United States

¹⁰ China Nuclear Data Center, China Institute of Atomic Energy, Beijing, China

¹¹ China University of Geosciences, Wuhan, China

¹² Chungbuk National University, Cheongju, Republic of Korea

¹³ Comenius University Bratislava, Faculty of Mathematics, Physics and Informatics, Bratislava, Slovak Republic

¹⁴ Creighton University, Omaha, Nebraska, United States

¹⁵ Department of Physics, Aligarh Muslim University, Aligarh, India

¹⁶ Department of Physics, Pusan National University, Pusan, Republic of Korea

¹⁷ Department of Physics, Sejong University, Seoul, Republic of Korea

¹⁸ Department of Physics, University of California, Berkeley, California, United States

¹⁹ Department of Physics, University of Oslo, Oslo, Norway

²⁰ Department of Physics and Technology, University of Bergen, Bergen, Norway

²¹ Dipartimento di Fisica, Università di Pavia, Pavia, Italy

²² Dipartimento di Fisica dell'Università and Sezione INFN, Cagliari, Italy

²³ Dipartimento di Fisica dell'Università and Sezione INFN, Trieste, Italy

²⁴ Dipartimento di Fisica dell'Università and Sezione INFN, Turin, Italy

²⁵ Dipartimento di Fisica e Astronomia dell'Università and Sezione INFN, Bologna, Italy

²⁶ Dipartimento di Fisica e Astronomia dell'Università and Sezione INFN, Catania, Italy

²⁷ Dipartimento di Fisica e Astronomia dell'Università and Sezione INFN, Padova, Italy

²⁸ Dipartimento di Fisica dell'Università and Sezione INFN, Pisa, Italy

²⁹ Dipartimento di Fisica 'E.R. Caianiello' dell'Università and Gruppo Collegato INFN, Salerno, Italy

³⁰ Dipartimento DISAT del Politecnico and Sezione INFN, Turin, Italy

³¹ Dipartimento di Scienze MIFT, Università di Messina, Messina, Italy

- ³² Dipartimento Interateneo di Fisica ‘M. Merlin’ and Sezione INFN, Bari, Italy
³³ European Organization for Nuclear Research (CERN), Geneva, Switzerland
³⁴ Faculty of Electrical Engineering, Mechanical Engineering and Naval Architecture, University of Split, Split, Croatia
³⁵ Faculty of Nuclear Sciences and Physical Engineering, Czech Technical University in Prague, Prague, Czech Republic
³⁶ Faculty of Physics, Sofia University, Sofia, Bulgaria
³⁷ Faculty of Science, P.J. Šafárik University, Košice, Slovak Republic
³⁸ Faculty of Technology, Environmental and Social Sciences, Bergen, Norway
³⁹ Frankfurt Institute for Advanced Studies, Johann Wolfgang Goethe-Universität Frankfurt, Frankfurt, Germany
⁴⁰ Fudan University, Shanghai, China
⁴¹ Gangneung-Wonju National University, Gangneung, Republic of Korea
⁴² Gauhati University, Department of Physics, Guwahati, India
⁴³ Helmholtz-Institut für Strahlen- und Kernphysik, Rheinische Friedrich-Wilhelms-Universität Bonn, Bonn, Germany
⁴⁴ Helsinki Institute of Physics (HIP), Helsinki, Finland
⁴⁵ High Energy Physics Group, Universidad Autónoma de Puebla, Puebla, Mexico
⁴⁶ Horia Hulubei National Institute of Physics and Nuclear Engineering, Bucharest, Romania
⁴⁷ HUN-REN Wigner Research Centre for Physics, Budapest, Hungary
⁴⁸ Indian Institute of Technology Bombay (IIT), Mumbai, India
⁴⁹ Indian Institute of Technology Indore, Indore, India
⁵⁰ INFN, Laboratori Nazionali di Frascati, Frascati, Italy
⁵¹ INFN, Sezione di Bari, Bari, Italy
⁵² INFN, Sezione di Bologna, Bologna, Italy
⁵³ INFN, Sezione di Cagliari, Cagliari, Italy
⁵⁴ INFN, Sezione di Catania, Catania, Italy
⁵⁵ INFN, Sezione di Padova, Padova, Italy
⁵⁶ INFN, Sezione di Pavia, Pavia, Italy
⁵⁷ INFN, Sezione di Pisa, Pisa, Italy
⁵⁸ INFN, Sezione di Torino, Turin, Italy
⁵⁹ INFN, Sezione di Trieste, Trieste, Italy
⁶⁰ Inha University, Incheon, Republic of Korea
⁶¹ Institute for Gravitational and Subatomic Physics (GRASP), Utrecht University/Nikhef, Utrecht, Netherlands
⁶² Institute of Experimental Physics, Slovak Academy of Sciences, Košice, Slovak Republic
⁶³ Institute of Physics, Homi Bhabha National Institute, Bhubaneswar, India
⁶⁴ Institute of Physics of the Czech Academy of Sciences, Prague, Czech Republic
⁶⁵ Institute of Space Science (ISS), Bucharest, Romania
⁶⁶ Institut für Kernphysik, Johann Wolfgang Goethe-Universität Frankfurt, Frankfurt, Germany
⁶⁷ Instituto de Ciencias Nucleares, Universidad Nacional Autónoma de México, Mexico City, Mexico
⁶⁸ Instituto de Física, Universidade Federal do Rio Grande do Sul (UFRGS), Porto Alegre, Brazil
⁶⁹ Instituto de Física, Universidad Nacional Autónoma de México, Mexico City, Mexico
⁷⁰ iThemba LABS, National Research Foundation, Somerset West, South Africa
⁷¹ Jeonbuk National University, Jeonju, Republic of Korea
⁷² Johann-Wolfgang-Goethe Universität Frankfurt Institut für Informatik, Fachbereich Informatik und Mathematik, Frankfurt, Germany
⁷³ Korea Institute of Science and Technology Information, Daejeon, Republic of Korea
⁷⁴ Laboratoire de Physique Subatomique et de Cosmologie, Université Grenoble-Alpes, CNRS-IN2P3, Grenoble, France
⁷⁵ Lawrence Berkeley National Laboratory, Berkeley, California, United States
⁷⁶ Lund University Department of Physics, Division of Particle Physics, Lund, Sweden
⁷⁷ Nagasaki Institute of Applied Science, Nagasaki, Japan
⁷⁸ Nara Women’s University (NWU), Nara, Japan
⁷⁹ National and Kapodistrian University of Athens, School of Science, Department of Physics , Athens, Greece
⁸⁰ National Centre for Nuclear Research, Warsaw, Poland
⁸¹ National Institute of Science Education and Research, Homi Bhabha National Institute, Jatni, India
⁸² National Nuclear Research Center, Baku, Azerbaijan

- ⁸³ National Research and Innovation Agency - BRIN, Jakarta, Indonesia
⁸⁴ Niels Bohr Institute, University of Copenhagen, Copenhagen, Denmark
⁸⁵ Nikhef, National institute for subatomic physics, Amsterdam, Netherlands
⁸⁶ Nuclear Physics Group, STFC Daresbury Laboratory, Daresbury, United Kingdom
⁸⁷ Nuclear Physics Institute of the Czech Academy of Sciences, Husinec-Řež, Czech Republic
⁸⁸ Oak Ridge National Laboratory, Oak Ridge, Tennessee, United States
⁸⁹ Ohio State University, Columbus, Ohio, United States
⁹⁰ Physics department, Faculty of science, University of Zagreb, Zagreb, Croatia
⁹¹ Physics Department, Panjab University, Chandigarh, India
⁹² Physics Department, University of Jammu, Jammu, India
⁹³ Physics Program and International Institute for Sustainability with Knotted Chiral Meta Matter (WPI-SKCM²), Hiroshima University, Hiroshima, Japan
⁹⁴ Physikalisches Institut, Eberhard-Karls-Universität Tübingen, Tübingen, Germany
⁹⁵ Physikalisches Institut, Ruprecht-Karls-Universität Heidelberg, Heidelberg, Germany
⁹⁶ Physik Department, Technische Universität München, Munich, Germany
⁹⁷ Politecnico di Bari and Sezione INFN, Bari, Italy
⁹⁸ Research Division and ExtreMe Matter Institute EMMI, GSI Helmholtzzentrum für Schwerionenforschung GmbH, Darmstadt, Germany
⁹⁹ Saga University, Saga, Japan
¹⁰⁰ Saha Institute of Nuclear Physics, Homi Bhabha National Institute, Kolkata, India
¹⁰¹ School of Physics and Astronomy, University of Birmingham, Birmingham, United Kingdom
¹⁰² Sección Física, Departamento de Ciencias, Pontificia Universidad Católica del Perú, Lima, Peru
¹⁰³ Stefan Meyer Institut für Subatomare Physik (SMI), Vienna, Austria
¹⁰⁴ SUBATECH, IMT Atlantique, Nantes Université, CNRS-IN2P3, Nantes, France
¹⁰⁵ Sungkyunkwan University, Suwon City, Republic of Korea
¹⁰⁶ Suranaree University of Technology, Nakhon Ratchasima, Thailand
¹⁰⁷ Technical University of Košice, Košice, Slovak Republic
¹⁰⁸ The Henryk Niewodniczanski Institute of Nuclear Physics, Polish Academy of Sciences, Cracow, Poland
¹⁰⁹ The University of Texas at Austin, Austin, Texas, United States
¹¹⁰ Universidad Autónoma de Sinaloa, Culiacán, Mexico
¹¹¹ Universidade de São Paulo (USP), São Paulo, Brazil
¹¹² Universidade Estadual de Campinas (UNICAMP), Campinas, Brazil
¹¹³ Universidade Federal do ABC, Santo Andre, Brazil
¹¹⁴ Universitatea Nationala de Stiinta si Tehnologie Politehnica Bucuresti, Bucharest, Romania
¹¹⁵ University of Derby, Derby, United Kingdom
¹¹⁶ University of Houston, Houston, Texas, United States
¹¹⁷ University of Jyväskylä, Jyväskylä, Finland
¹¹⁸ University of Kansas, Lawrence, Kansas, United States
¹¹⁹ University of Liverpool, Liverpool, United Kingdom
¹²⁰ University of Science and Technology of China, Hefei, China
¹²¹ University of South-Eastern Norway, Kongsberg, Norway
¹²² University of Tennessee, Knoxville, Tennessee, United States
¹²³ University of the Witwatersrand, Johannesburg, South Africa
¹²⁴ University of Tokyo, Tokyo, Japan
¹²⁵ University of Tsukuba, Tsukuba, Japan
¹²⁶ Universität Münster, Institut für Kernphysik, Münster, Germany
¹²⁷ Université Clermont Auvergne, CNRS/IN2P3, LPC, Clermont-Ferrand, France
¹²⁸ Université de Lyon, CNRS/IN2P3, Institut de Physique des 2 Infinis de Lyon, Lyon, France
¹²⁹ Université de Strasbourg, CNRS, IPHC UMR 7178, F-67000 Strasbourg, France, Strasbourg, France
¹³⁰ Université Paris-Saclay, Centre d'Etudes de Saclay (CEA), IRFU, Département de Physique Nucléaire (DPhN), Saclay, France
¹³¹ Université Paris-Saclay, CNRS/IN2P3, IJCLab, Orsay, France
¹³² Università degli Studi di Foggia, Foggia, Italy
¹³³ Università del Piemonte Orientale, Vercelli, Italy
¹³⁴ Università di Brescia, Brescia, Italy
¹³⁵ Variable Energy Cyclotron Centre, Homi Bhabha National Institute, Kolkata, India

¹³⁶ Warsaw University of Technology, Warsaw, Poland

¹³⁷ Wayne State University, Detroit, Michigan, United States

¹³⁸ Yale University, New Haven, Connecticut, United States

¹³⁹ Yildiz Technical University, Istanbul, Turkey

¹⁴⁰ Yonsei University, Seoul, Republic of Korea

¹⁴¹ Affiliated with an institute formerly covered by a cooperation agreement with CERN

¹⁴² Affiliated with an international laboratory covered by a cooperation agreement with CERN.